SKB

TECHNICAL REPORT 91-33

Transient nuclide release through the bentonite barrier – SKB 91

Akke Bengtsson, Hans Widén

Kemakta Konsult AB

May 1991

SVENSK KÄRNBRÄNSLEHANTERING AB
SWEDISH NUCLEAR FUEL AND WASTE MANAGEMENT CO

BOX 5864 S-102 48 STOCKHOLM

TEL 08-665 28 00 TELEX 13108 SKB S
TELEFAX 08-661 57 19

TRANSIENT NUCLIDE RELEASE THROUGH THE BENTONITE BARRIER - SKB91

Akke Bengtsson, Hans Widén

Kemakta Konsult AB

May 1991

Transient nuclide release through the bentonite barrier - SKB91

Authors:
Akke Bengtsson
Hans Widén

Kemakta Konsult AB
May 1991

ABSTRACT

A study of near-field radionuclide migration is presented. The study has been performed in the context of the SKB91 study which is a comprehensive performance assessment of disposal of spent fuel. The objective of the present study has been to enable the assessment of which nuclides can be screened out because they decay to insignificant levels already in the near-field of the repository.

A numerical model has been used which describes the transient transport of radionuclides through a small hole in a HLW canister imbedded in bentonite clay into a fracture in the rock outside the bentonite. Calculations for more than twenty nuclides, nuclides with both high and low solubility, have been made. The effect of sorption in the bentonite backfill is included. The size of the penetration hole was assumed to be constant up to time when the calculations were terminated, 500 000 years after the deposition. The mass transport rate is controlled by diffusion. The model is three dimensional.

The report describes the geometry of the modelled system, the assumptions concerning the transport resistances at the boundary conditions, the handling of the source term and obtained release curves.

CONTENTS

1 MODEL DESCRIPTION

A simplified scenario of instationary diffusion through a cylindrical bentonite barrier has been studied. The diffusion takes place from a small hole in the spent fuel canister to a fracture with flowing water in the host rock. Both simple analytical estimates of the maximum release rates at steady state and numerical calculations of the instationary diffusion has been made. The numerical modelling of the instationary diffusion is made with the Integrated Finite Differences computer code TRUCHN. An extended version of the heat transport code TRUMP. (Edwards, 1969)

1.1 The canister and deposition hole geometry

The sides of the deposition hole are lined with blocks of dry compacted bentonite with a plug of bentonite at the bottom. The copper canister with spent fuel is lowered into the pit and a plug of compacted bentonite put on top of it. Some time after the closure of the repository, the bentonite blocks are assumed to be soaked with water and swelled to form a monolithic barrier around the copper canister. The dimensions of the deposition hole and canister are shown in Table 1-1.

The mantle surface of the bentonite barrier is intersected by a fracture plane in the surrounding rock. It is assumed that the canister shell is penetrated by a small hole. The hole is assumed to be in the same plane as the fracture plane in the surrounding rock. (See Figure 1-1)

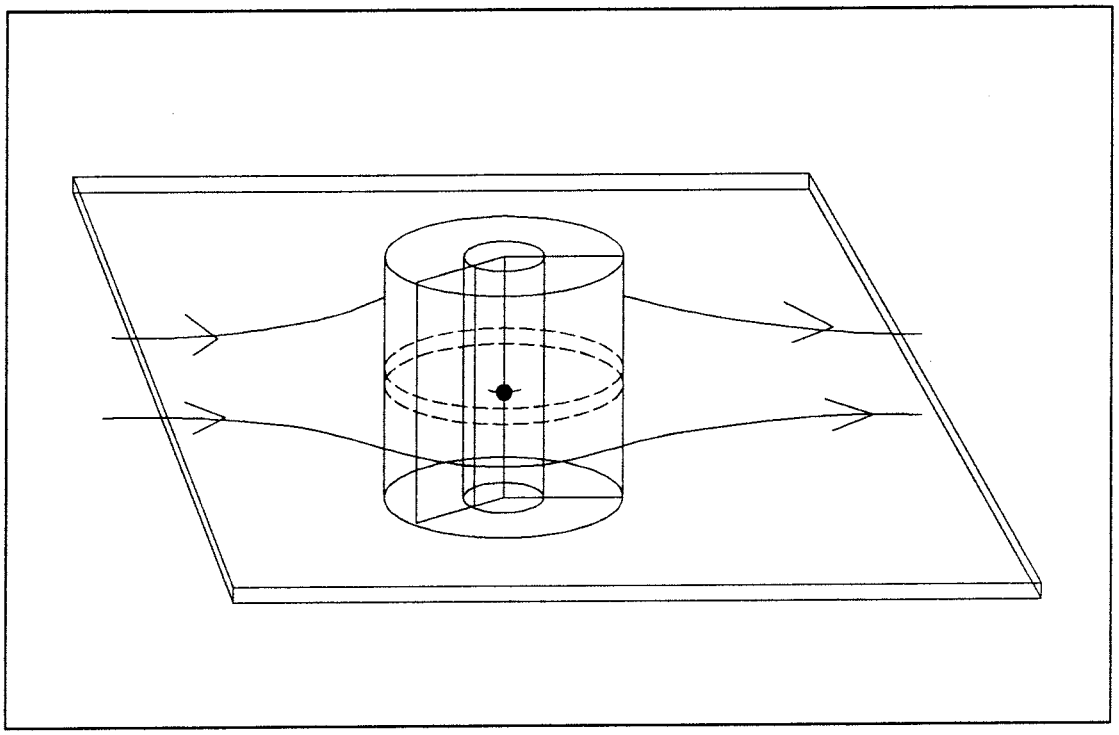

Figure 1-1
Modelled part of the bentonite barrier.
(For the sake of clarity the proportions in the figure are not correct.
See Table 1-1 for the exact values.)

The migration path between the hole in the canister and the fracture mouth in the rock is modeled as a slab of bentonite instead of a cylindrical shell. The modelled slab has an area of 1x1 m with the canister hole in the center and a thickness of 0.35 m (See Figure 1-2). This corresponds to a section of a cylindrical shell with a height of 1 m and about a third of the circumference of the bentonite mantle (See Figure 1-1). The parts of the bentonite barrier outside this sector will not materially contribute to the transport from the canister to the fracture in the rock and the approximation made in flattening out this limited part of the shell is also small.

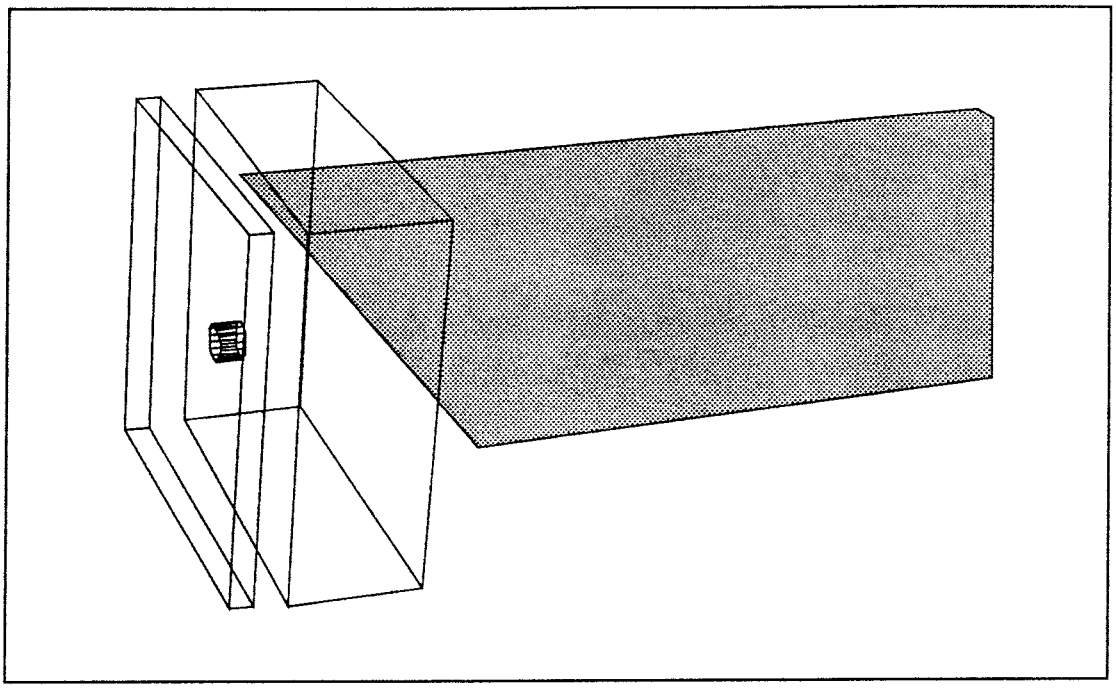

Figure 1-2
Plane parallel realisation of the cylindrical diffusion geometry.

Table 1-1
The bentonite barrier. Dimensions of important features.

Outer diameter of canister	0.75 m
Thickness of bentonite barrier	0.35 m
Hole in canister wall	5.0 mm^2
Fracture aperture	0.5 mm
Height of modelled section	1 m

1.2 Nuclide inventory

The whole radionuclide inventory is assumed to be available for dissolution at the time a migration path forms through the spent fuel canister shell. This is a conservative way of describing the canister leach process which not is connected to any particular fuel dissolution rate. Because of the limited void space inside the canister, the solubility limit will be exceeded though for a number of the nuclides studied. In the present study, the solubility limits are assigned all isotopes of a certain molecular specie. This approach overestimates the release rates of species with several isotopes, (for instance Pu). The time a solid phase exists depends on the radioactive decay rate and the transport rate out to the bentonite (See Section 2.4)

Table 1-2
Nuclide inventory at start of release.

Nuclide	Halflife [years]	Initial amount [mol]
C-14	5.73e+03	0.02
Cl-36	3.00e+05	0.035
Ni-59	7.60e+04	0.92
Ni-63	1.00e+02	0.13
Se-79	6.50e+04	0.12
Sr-90	2.80e+01	4
Zr-93	1.50e+06	13.5
Nb-94	2.00e+04	0.01
Tc-99 ox	2.10e+05	12.4
Tc-99 red	2.10e+05	12.4
Pd-107	6.50e+06	3.4
Sn-126	1.00e+05	0.36
I-129	1.60e+07	2.2
Cs-135	3.00e+06	4.6
Cs-137	3.00e+01	6.2
Ce-142	2.00e+11	12.8
Sm-151	9.00e+01	0.1
Np-237	2.10e+06	10.2
Pu-238	8.80e+01	0.88
Pu-239	2.41e+04	28.1
Pu-240	6.56e+03	14.8
Pu-242	3.80e+05	3.3
Am-241	4.32e+02	6.6
Am-243	7.37e+03	0.73

1.3 The bentonite

The properties used are for a sodium bentonite, Wyoming MX-80, compacted to a wet bulk density of 2000 kg/m^3. The parameter values primarily used are nuclide dependent effective- and apparent diffusivity. The values are taken from a critical evaluation of experimental data made by Brandberg and Skagius, 1991. The experimental data behind were for the effective diffusivities derived from steady-state transport rates through a slab with a fixed concentration difference across. The D_a-values used are calculated from penetration data into a body of bentonite.

An apparent diffusivity is otherwise often calculated as a function of effective diffusivity, diffusion porosity and mass sorption coefficient as:

$$D_a = D_e\left(\frac{1}{\varepsilon_p + K_d \rho_p}\right) \qquad (1\text{-}1)$$

where the mass sorption coefficient for instance is derived from experiments where a known amount of nuclide is equilibrated with a bentonite slurry and the resulting concentration in the free water is measured. The so calculated apparent diffusivities are not always consistent with the values derived from instationary penetration experiments.

Where K_d-values have been utilised in this study, they have been back-calculated from the experimental D_a-values using (1-1). The so calculated K_d-values are for Pu a factor 10 higher than the values derived from experiments in which a solution with a known amount of nuclide is equilibrated with a bentonite slurry. (Brandberg and Skagius, 1991). In the instationary transport calculations however, the D_a-values are used, thereby circumventing the inconsistency.

The diffusion porosity ε_p is assumed to be 0.25 for all nuclides except for the anions of Cl, I and Tc (under oxidising conditions) where it is assumed to be 0.05.

Table 1-3
Nuclide dependent bentonite data. (Brandberg and Skagius, 1991)
(For the shadowed column, see section 1.3)

	D_e [m^2/a]	D_a [m^2/a]	ε_p	K_d [m^3/kg]
C-14	3.20e-03	1.28e-02	0.25	0
Cl-36	7.90e-05	1.58e-03	0.05	0
Ni-59	3.20e-03	3.20e-06	0.25	0.5
Ni-63	3.20e-03	3.20e-06	0.25	0.5
Se-79	3.20e-03	5.12e-04	0.25	0.003
Sr-90	7.90e-01	3.90e-02	0.25	0.01
Zr-93	3.20e-03	8.00e-07	0.25	2
Nb-94	3.20e-03	8.00e-06	0.25	0.2
Tc-99 ox	7.90e-05	1.58e-03	0.05	0
Tc-99 red	7.90e-05	3.95e-07	0.25	0.1
Pd-107	3.20e-03	1.58e-04	0.25	0.01
Sn-126	3.20e-03	5.33e-07	0.25	3
I-129	7.90e-05	1.58e-03	0.05	0
Cs-135	7.90e-01	7.88e-03	0.25	0.05
Cs-137	7.90e-01	7.88e-03	0.25	0.05
Ce-142	3.20e-03	1.60e-06	0.25	1
Sm-151	3.20e-03	1.60e-06	0.25	1
Np-237	3.20e-03	5.33e-07	0.25	3
Pu-238	3.20e-03	3.20e-08	0.25	50
Pu-239	3.20e-03	3.20e-08	0.25	50
Pu-240	3.20e-03	3.20e-08	0.25	50
Pu-242	3.20e-03	3.20e-08	0.25	50
Am-243	3.20e-03	5.33e-07	0.25	3
Am-241	3.20e-03	5.33e-07	0.25	3

2 INITIAL CALCULATIONS UTILISING STEADY STATE CONDITIONS

2.1 Use of steady state solutions

Solutions for steady state conditions have been utilised both in calculating the source term and the discretisation for the non steady state calculations. Steady state diffusion solutions also have been used to calculate conservative limits for the release rates through the bentonite barrier.

The main concentration drop along the migration path from the hole in the canister to the fracture mouth in the host rock takes place in two small volumes adjacent to the start and end point. The time to reach steady state across these zones are short compared to the time scale for the diffusion through the whole bentonite barrier. These parts of the migration path through the bentonite barrier could therefore conveniently be modeled as steady state diffusion resistances.

The mass flow rate at steady state through such a zone could be expressed as:

$$\dot{N} = Q_{eq} \cdot \Delta C \tag{2-1}$$

where ΔC is the concentration drop across the zone.

In the following two chapters will be shown how to calculate the equivalent water flow rate Q_{eq} for spherical- and cylindrical geometry.

2.2 Diffusion from a hole into a semi infinite medium

The mass transfer resistance at steady state for the part of the bentonite closest to the hole in the canister surface is calculated in the following way:

The concentration profile in a spherical shell with inner radius a and outer radius b with the concentrations C_a at $r=a$ and C_b at $r=b$ is given by:

$$C(r) = \frac{aC_a}{r} + \frac{(bC_b - aC_a)(r-a)}{r(b-a)} \tag{2-2}$$

(Adaption of Equation 1 at page 246 of Carslaw&Jaeger for $t\rightarrow\infty$)
If $(C_a - C_b) = \Delta C$, the diffusive transport rate through a conical sector with a solid angle of θ steradians is given by:

$$\dot{N} = -r^2\theta D_e\left(\frac{\partial C}{\partial r}\right) = \theta D_e \Delta C \frac{ab}{(b-a)} \tag{2-3}$$

and as a consequence:

$$Q_{eq} = \frac{D_e\theta ab}{(b-a)} \tag{2-4}$$

Because of the input data structure for the instationary transport code we want to express the equivalent water flow rate as a product of an area A and a mass transfer coefficient α. The area of a sector of a spherical surface with radius r and center angle θ is then:

$$A = \theta r^2 \tag{2-5}$$

and the mass transfer coefficient:

$$\alpha = D_e \frac{ab}{r^2(b-a)} \tag{2-6}$$

An observandum is that for a sector of a spherical shell with $b>>a$, Q_{eq} approaches:

$$Q_{eq,\infty} = \theta D_e a \tag{2-7}$$

which is independent of b.

A plot of $1/Q_{eq}$ vs. b for a value of a giving an area of 5 mm^2 (the size of the hole in the canister wall) is shown in Figure 2-1. As can be seen from the plot, a major part of the total diffusion resistance at steady state lies in the first cm of bentonite.

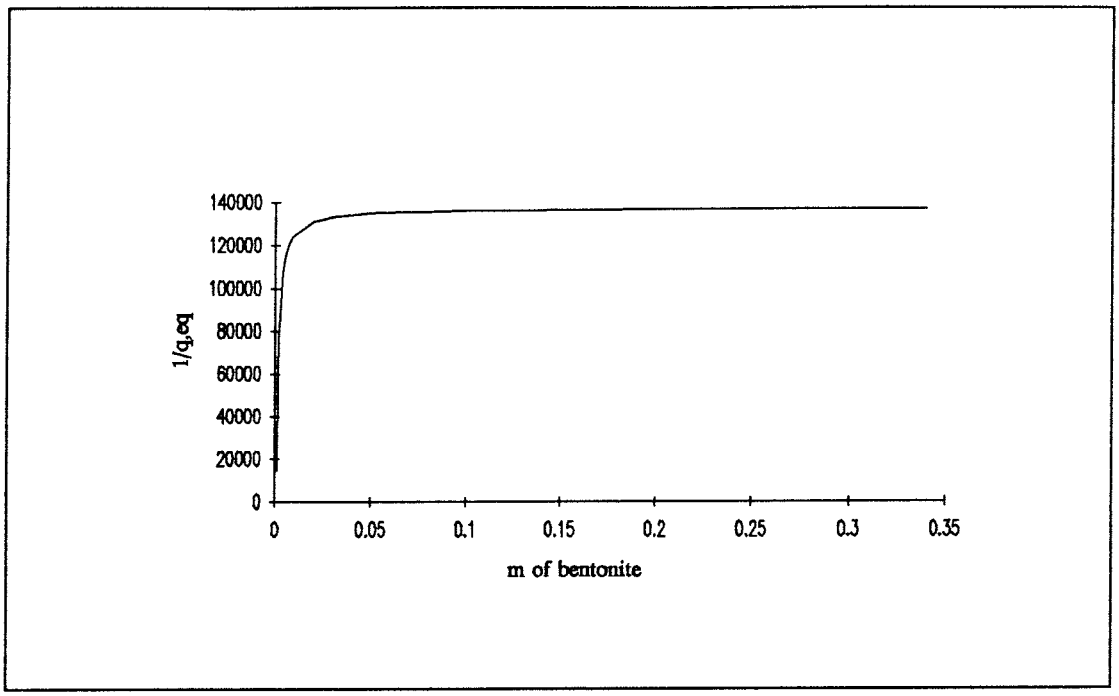

Figure 2-1
Mass transfer resistance at steady state of bentonite adjacent to 5 mm^2 hole.

2.3 Diffusion to a slit in a semi infinite medium

The mass transfer resistance at steady state for the part of the bentonite closest to the intersection of the external surface of the bentonite barrier and a fracture plane in the host rock is calculated in the following way:

The concentration profile in a hollow cylinder with inner radius a, outer radius b with a concentration C_b outside and C_a inside will be:

$$C(r) = \frac{C_a \ln(b/r) + C_b \ln(r/a)}{\ln(b/a)} \tag{2-8}$$

(This equation and the next are slightly rewritten forms of Equations 3 and 4, page 189 of Carslaw and Jaeger, 1959.)

If $(C_b - C_a) = \Delta C$, the mass flow rate through a wedge with center angle ϕ and length l is:

$$\dot{N} = -\phi r l \, D_e \frac{dC}{dr} = \frac{\phi l D_e \Delta C}{\ln\left(\frac{b}{a}\right)} \tag{2-9}$$

$$Q_{eq} = \frac{\phi l D_e}{\ln\left(\frac{b}{a}\right)} \tag{2-10}$$

Even in this case the plot of $1/Q_{eq}$ vs. b shows that the major concentration drop takes place in the immediate vicinity of the fracture aperture. (cf. Figure 2-2) As can be seen from the equations, Q_{eq} for the cylinder however does not approach an assymptotic value for large values of b.

In the same way as for the spherical shell we could split Q_{eq} into a product of an area and a mass transfer coefficient.
The mantle area of a sector of a cylinder with the length l, radius r and center angle ϕ is:

$$A = r\phi l \tag{2-11}$$

which gives a mass transfer coefficient:

$$\alpha = \frac{D_e}{r \cdot \ln\frac{b}{a}} \tag{2-12}$$

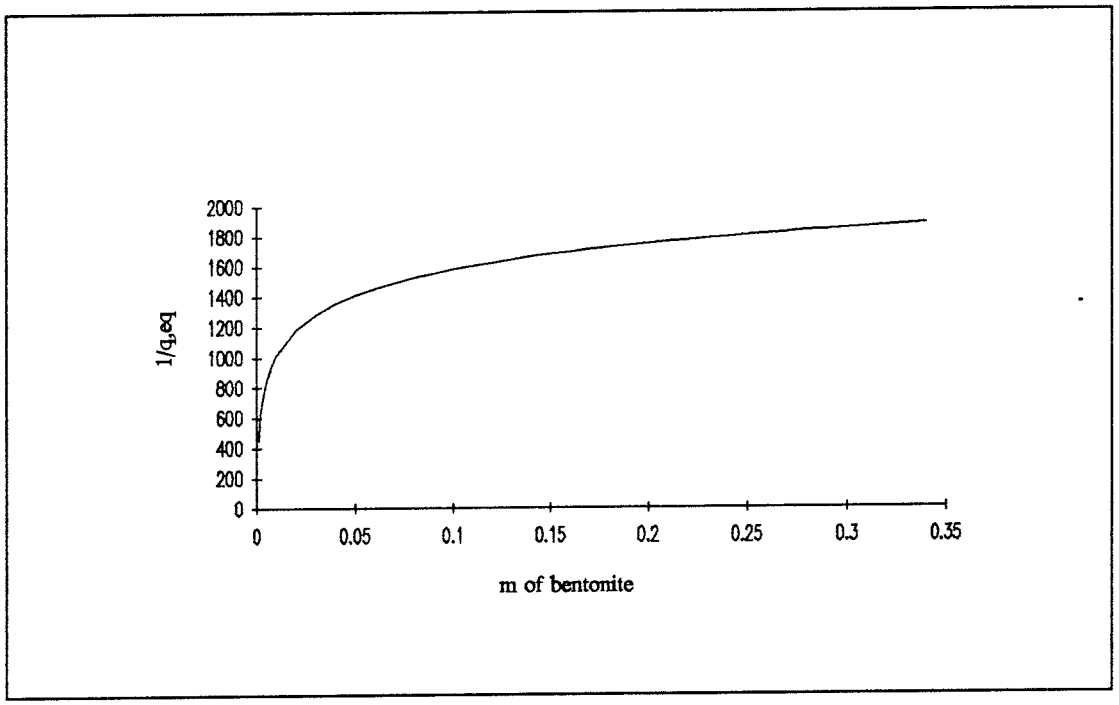

Figure 2-2
Mass transfer resistance at steady state of bentonite adjacent to a 1 m long slit with a width of 0.5 mm.

2.4 Leach rates from a spent fuel canister

All material inside a canister is assumed to be available for dissolution at time zero. The small water volume available to dissolve the material in is the canister internal void space = 0.02 m^3. As was shown in Section 2.2, the major concentration drop takes place across the first cm:s of bentonite. This means that after a short instationary phase the leach rate will be proportional to the concentration difference across the equilibrated bentonite layer with a proportionality constant Q_{eq}. The rate of change in the amount remaining in the canister will then be:

$$\frac{dN_{gap}}{dt} = -\lambda N_{gap} - Q_{eq} C_{gap} \tag{2-13}$$

Which for the non solubility limited nuclides equates to:

$$\frac{dN_{gap}}{dt} = -\lambda N_{gap} - \frac{Q_{eq} N_{gap}}{v_{gap}} \tag{2-14}$$

Integrating this using $N=N_0$ at $t=0$ gives the amount remaining as:

$$N_{gap} = N_0 e^{-\left(\lambda + \frac{Q_{eq}}{v_{gap}}\right)t} \tag{2-15}$$

The radioactive decay rate is smaller than the escape rate into the bentonite for all the non solubility limited nuclides studied.

For about half of the nuclides studied the solubility limit is reached and part of their inventory will remain as a solid phase for some time. An estimate of the time this solid phase exists could be made by assuming pseudo steady state diffusion through the first cm:s of bentonite closest to the hole in the canister wall.

As long as the solubility limit is reached the rate of decrease in amount remaining in the canister interstitial volume could be estimated with:

$$\frac{dN_{gap}}{dt} = -\lambda N_{gap} - Q_{eq} C_{sol} \tag{2-16}$$

using the assymptotic value of water flow rate $Q_{eq}=Q_{eq,\infty}$ for the bentonite adjacent to the hole in the canister as derived in Section 2.2.

As material escapes from the canister interstitial volume or decays more solid material dissolves until there is no more solid phase left at $t=t_{leach}$.
Integration of (2-16) using $N=N_0$ at $t=0$ gives:

$$N_{gap} = N_0 e^{-\lambda t} - (1 - e^{-\lambda t}) \frac{Q_{eq} C_{sol}}{\lambda} \tag{2-17}$$

t_{leach} could be calculated by setting $N_{gap}=C_{sol}v_{gap}$:

$$t_{leach} = \frac{1}{\lambda}\ln\left(\frac{\frac{N_0}{C_{sol}}+\frac{Q_{eq}}{\lambda}}{v_{gap}+\frac{Q_{eq}}{\lambda}}\right) \tag{2-18}$$

For $t>t_{leach}$ the interstitial concentration C_{gap} will no longer remain constant and the rate of change in the amount remaining in the gap will then be given by (2-14)
Integration of (2-14) using $N_{gap}=C_{sol}v_{gap}$ at $t=t_{leach}$ gives:

$$N_{gap} = C_{sol}v_{gap}e^{-\left(\lambda+\frac{Q_{eq}}{v_{gap}}\right)(t-t_{leach})} \tag{2-19}$$

Numerical integration of the inflow rate to the bentonite barrier calculated in the TRUCHN calculation and solving for $N_{gap}=C_{sol}v_{gap}$ gives a more correct value of t_{leach} which though for all nuclides is about the same as the values computed using (3-6).
There is just one potential pitfall. To simply do the numerical integration in explicit form like:

$$\Delta N_{gap}=-\lambda N_{gap}\Delta t-\dot{N}\Delta t \tag{2-20}$$

where N_{gap} on the right side is the value at the start of the time interval gives in inaccurate results as it overestimates the radioactive decay when the time interval is of the same order or larger than the half life of the nuclide. The time intervals are here the interval between successive printouts which for practical reasons easily could be larger than the half life.
Instead a slight modification of (2-17) has been used. By integrating (2-16) over the time interval Δt with the amount N_n at the start of the time interval we could express the amount left at the end of the time interval as:

$$N_{n+1} = N_n e^{-\lambda\Delta t}-(1-e^{-\lambda\Delta t})\frac{\dot{N}_n}{\lambda} \tag{2-21}$$

The integrated inflow rate from the IFD calculation of the instationary diffusion was calculated in this way and the time to reach $N_{gap}=C_{sol}v_{gap}$ very closely coincides with the values predicted by (2-19 and 2-18). The values of C_{sol} and t_{leach} are shown in Table 2-1.

Table 2-1
Gap concentrations and leaching times.

Nuclide	Solubility [mol/m^3]	t_{leach} [a]	Initial concentration [mol/m^3]
C-14	high		2.50e-01
Cl-36	high		4.38e-01
Ni-59	1.00e+00	3.88e+04	
Ni-63	1.00e+00	2.54e+02	
Se-79	1.00e-05	8.25e+05	
Sr-90	high		5.00e+01
Zr-93	3.00e-05	2.01e+07	
Nb-94	1.00e-05	2.15e+05	
Tc-99 ox	high		1.55e+02
Tc-99 red	2.00e-05	4.59e+06	
Pd-107	1.50e-03	2.45e+07	
Sn-126	2.00e-05	1.27e+06	
I-129	high		2.75e+01
Cs-135	high		5.75e+01
Cs-137	high		7.75e+01
Ce-142	1.00e-05	6.01e+10	
Sm-151	1.00e-05	1.69e+03	
Np-237	2.00e-06	3.45e+07	
Pu-238	2.00e-05	1.84e+03	
Pu-239	2.00e-05	5.05e+05	
Pu-240	2.00e-05	1.43e+05	
Pu-242	2.00e-05	5.30e+06	
Am-241	6.00e-05	9.38e+03	
Am-243	6.00e-05	1.16e+05	

2.5 Limiting values for the diffusion through the bentonite barrier

Comparing the Q_{eq}-values for the vicinity of the hole and the slit (see figures 2-1 and 2-2) we see that it is larger for the slit by a factor of about 100. This does not necessarily mean that the transport resistance close to the slit is unimportant. The mass transport rate is the product of the equivalent water flow rate and the maximum concentration drop over the zone in question. Particularly for the non solubility limited nuclides the concentration just before the last cm:s of bentonite will be significantly lower than the initial source concentration as the effective capacity of the bentonite exceeds the fuel canister gap volume even for the non sorbing nuclides.

An upper limit on the release of non solubility limited nuclides at the end of the bentonite barrier could be calculated using the equivalent water flow rate for the cm of bentonite closest to the fracture aperture with ΔC= the concentration in the bentonite for the hypothetical case where the initial inventory is spread out to the same concentration (C_{eq}) all throughout the bentonite barrier and zero concentration on the outside. (See table 2-2, columns 4 and 5)

For the nuclides for which the solubility limit is reached in the source (See section 2.4) the release rate at the end of the bentonite barrier will assymptotically approach an upper limit set by the solubility and the steady state mass transfer resistance of a spherical shell with an outer radius much larger than the inner. The equivalent water flow rate $Q_{eq,\infty}$ as calculated by Equation (2-7) is only about 8% lower than Q_{eq} for the first cm of bentonite. For many nuclides the actual release through the bentonite will never reach this value before the solid phase in the source is depleted. For nuclides with low solubility the amount remaining when the solid phase is depleted will be very small and the gap concentration will then drop very rapidly. The additional increase in release rate to the outside of the bentonite barrier will be very small and the release rate will also decrease rapidly after a time corresponding to the penetration time for diffusion through the bentonite. The assymptotic upper limit for the release rate of the solubility limited nuclides is shown in table 2-2, column 3.

For many of the nuclides with high sorption in the bentonite, the release through the bentonite barrier will still be increasing at the arbitrarily chosen end of calculation at 500,000 years and the release rates will later be shown to be often much lower than the assymptotic value calculated here. See also the discussion concerning alternative release paths in Section 4.1 and 4.3.

Table 2-2
Upper limits for the release rates because of the diffusion area restriction close to the hole and the fracture aperture.

	$Q_{eq,\infty}$	$Q_{eq,\infty}*C_{sol}$	C_{eq}	$Q_{eq,slit}*C_{eq}$
	[m^3/a]	[mol/a]	[mol/m^3]	[mol/a]
C-14			1.86e-01	4.27e-04
Cl-36			9.33e-01	5.29e-05
Ni-59	1.79e-05	1.79e-05		
Ni-63	1.79e-05	1.79e-05		
Se-79	1.79e-05	1.79e-10		
Sr-90			5.63e-01	3.19e-01
Zr-93	1.79e-05	5.38e-10		
Nb-94	1.79e-05	1.79e-10		
Tc-99 ox			3.31e+02	1.87e-02
Tc-99 red	4.43e-07	8.86e-12		
Pd-107	1.79e-05	2.69e-08		
Sn-126	1.79e-05	3.59e-10		
I-129			5.87e+01	3.32e-03
Cs-135			1.31e-01	7.42e-02
Cs-137			1.77e-01	1.00e-01
Ce-142	1.79e-05	1.79e-10		
Sm-151	1.79e-05	1.79e-10		
Np-237	1.79e-05	3.59e-11		
Pu-238	1.79e-05	3.59e-10		
Pu-239	1.79e-05	3.59e-10		
Pu-240	1.79e-05	3.59e-10		
Pu-242	1.79e-05	3.59e-10		
Am-241	1.79e-05	1.08e-09		
Am-243	1.79e-05	1.08e-09		

3 INSTATIONARY DIFFUSION THROUGH THE BENTONITE

3.1 Discretisation for the Integrated Finite Differences calculations.

Because of symmetry only a quarter of the 1X1 m bentonite slab needs to be modelled. See Figure 3-1. This 0.5X0.5X0.35 m slab with one corner at the center of the hole in the canister is discretised in the following way starting at that corner. The coordinate axises have origo in the center of the hole in the canister. The Z-axis goes from the hole into the bentonite to the fracture. The X- and Y-axises lie in the plane of the inner surface of the bentonite barrier with the X-axis parallel to the fracture.

- Along the X- and Y-axis: 15 nodes from 0.0 to 0.5 m, initial node length 0.01 m, node lengths in geometric progression with each node length 1.156 of the preceding.

- Along the Z-axis: 10 nodes from 0.0 to 0.17 m, initial node length 0.01 m, node lengths in geometric progression with each node length 1.11 of the preceding.
  10 nodes from 0.17 to 0.35 m, final node length 0.01 m, node lengths in geometric progression with each node length 0.88 of the preceding.

3.2 Initial and boundary conditions

- Initial conditions

Zero concentration everywhere in the bentonite except for the non solubility limited nuclides for which a node with the volume v_{gap} is assigned the concentration $C=N_0/v_{gap}$.

- Boundary conditions, general

The node with the corner at the hole in the canister and the row of nodes with an edge along the host rock fracture aperture (see figure 3-1) are replaced with connections to the respective in- and output boundary conditions. The mass transfer resistance of these boundary connections equals the mass transfer resistance through the excluded volumes at steady state. (See Chapter 2.)

The diffusion resistance through the node adjacent to the hole in the canister is calculated as for a hollow sphere. (Cf Section 2.2) A surface area of a hemisphere equal to the area of the hole in the canister wall (5 mm^2) gives an inner radius of the spherical shell of 0.892 mm. The outer surface area of the quarter of the hemisphere actually modeled is the sum of the three 1cmX1cm interface areas to the adjacent nodes which gives an outer radius of 1.38 cm.
The diffusion resistances for the nodes adjacent to the fracture aperture in the host rock is calculated as for a hollow cylinder. (Cf Section 2.3) An inner area of a half cylinder giving the same area per unit of length as the host rock fracture aperture (0.5 mm) gives an inner radius of the equivalent hollow cylinder of 0.159 mm. The outer surface area per unit of length of the 90° sector of the cylinder actually modelled is equal to the sum of the two 1 cm wide interface areas to the adjacent nodes which gives an outer radius of 1.27 cm.

The capacity of the volumes excluded are neglected but this is a minor approximation as the excluded volumes represent less than 0.06 percent of the total capacity

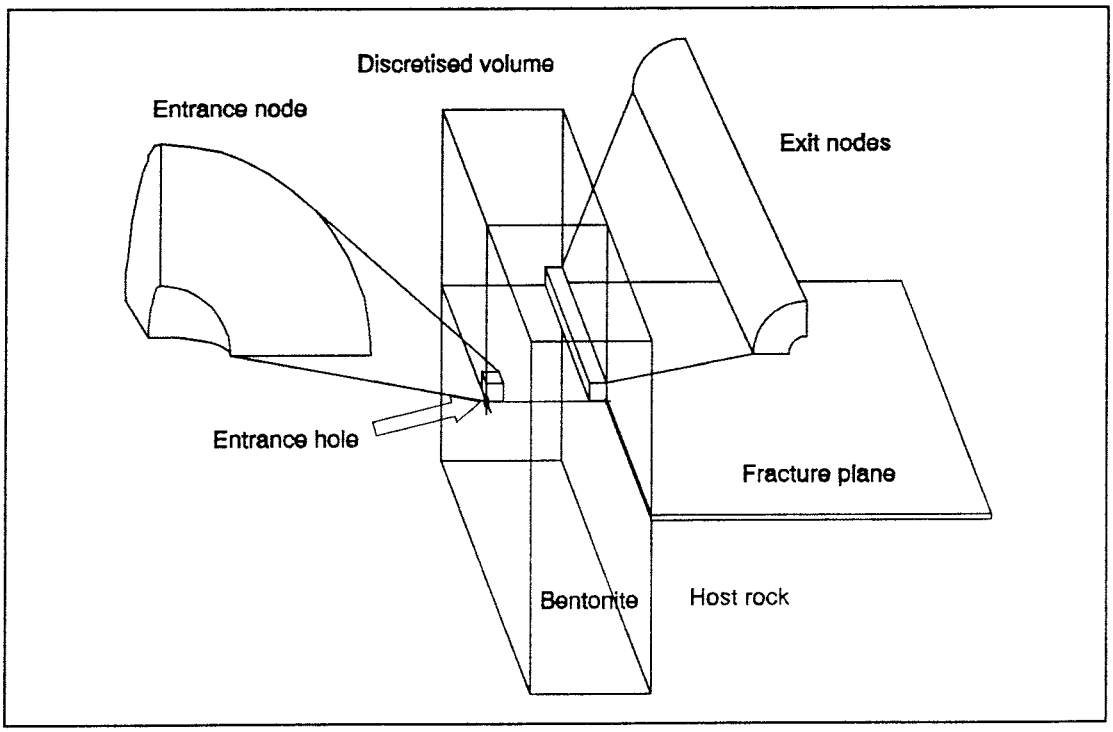

Figure 3-1
The in- and output boundary nodes.

The mass transfer resistance of a film resistance type boundary connection can be expressed in terms of an equivalent water flow rate Q_{eq} equal to the product of an area and a mass transfer coefficient. The equivalent water flow rate for diffusion through a spherical or cylindrical shell at steady state is independent of radius but as a boundary connection in TRUCHN is described by the product of an area and a mass transfer coefficient a radius has to be chosen. A convenient choice was to use radius corresponding to the outer radius of the equivalent spherical or cylindrical shell as described above as the resulting area already is calculated during the discretisation. Then the mass transfer coefficient can be calculated as shown in Equations 2-6 and 2-12 respectively and written into the TRUCHN input data.

Input boundary condition for solubility limited nuclides

Up to $t=t_{leach}$ a film resistance type boundary condition as described above.
After t_{leach} the input boundary condition is removed. (An isolated boundary condition and not, as often is used, just setting the boundary concentration to zero which gives an unphysical and often quite significant backwards diffusion.)
For Ni-59 and Ni-63 a substantial part of the initial inventory still remains after the solid phase is depleted. The amount remaining ($N_{gap}=C_{sol}v_{gap}$) is collected in a node simulating the canister interstitial volume coupled to the rest of the node net using a radiative connection in the same way as for $t<t_{leach}$. For all other nuclides the amount remaining at $t=t_{leach}$ will not significantly contribute to the release rate at the outside of the bentonite barrier.

- Input boundary condition for non solubility limited nuclides

The node representing the canister gap volume is coupled to the rest of the node net. It is coupled to the rest of the node net through a film resistance type connection through the three 1 cm^2 surfaces in an analogous way as discussed above for the input boundary condition for solubility limited nuclides. No other input boundary condition is specified.

Output boundary condition

Zero concentration coupled through a film resistance type boundary condition as described above. (In variation discussed in Section 4.2, film resistance in the fracture is added but still the boundary concentration is zero.

3.3 Instationary release through the bentonite barrier

The solubility- and non solubility limited nuclides give distinctly different results. A larger fraction of the initial inventory is rapidly released from the canister to the bentonite for the non solubility limited nuclides. As they also all are weakly sorbed or not sorbed at all in the bentonite the penetration through the bentonite is also very rapid and most of the initial inventory eventually escapes through the bentonite before decaying.

For the solubility limited nuclides, the results are very sensitive to the balance between the time to penetrate the bentonite barrier and the time to deplete the solid phase which in its turn depends on the solubility. The build up of the release rate to the host rock fracture rapidly ends when the solid phase is depleted. For a number of the more strongly sorbing nuclides the penetration through the bentonite is so slow that the release rate still is far below the maximum and rising when the calculation was terminated at 500,000 years.
The results of the calculations are summarised in Table 3-1. Figures of release rates and integrated released fraction as a function of time are supplied in Appendix A.

Table 3-1
Instationary release through the bentonite barrier.

Nuclide	Maximum release rate	t(max. rate)	Released fraction at $5 \cdot 10^5$ years	Remaining in gap	Remaining in gap +bentonite
	Mol/year	years		fraction	fraction
C-14	1.46e-05	1.80e+02	8.78e-01	0.00	1.54e-05
Cl-36	7.18e-07	2.20e+03	9.06e-01	0.00	1.83e-06
Ni-59	2.41e-06	4.50e+04	2.46e-01	0.00	4.00e-04
Ni-63	2.01e-13	1.20e+03	1.25e-09	0.00	1.54e-10
Se-79	1.72e-10	>5e5	7.15e-04	4.72e-03	4.72e-03
Sr-90	1.02e-01	6.50e+00	5.98e-01	0.00	2.70e-05
Zr-93	1.85e-10	>5e5	3.89e-06	7.93e-01	7.93e-01
Nb-94	3.92e-11	2.17e+05	8.56e-04	0.00	2.32e-09
Tc-99,ox	2.57e-04	2.30e+03	8.71e-01	0.00	1.00e-06
Tc-99,red	9.65e-13	>5e5	2.49e-08	1.92e-01	1.92e-01
Pd-107	2.63e-08	>5e5	3.82e-03	9.44e-01	9.44e-01
Sn-126	2.99e-11	>5e5	3.10e-05	3.11e-02	3.14e-02
I-129	4.51e-05	2.20e+03	9.99e-01	0.00	5.41e-06
Cs-135	4.19e-02	1.05e+01	1.02e+00	0.00	8.65e-05
Cs-137	4.56e-02	8.00e+00	2.82e-01	0.00	1.89e-04
Ce-142	1.09e-10	>5e5	2.50e-06	1.00e+00	1.00e+00
Sm-151	4.86e-21	2.30e+03	8.75e-17	0.00	1.94e-18
Np-237	9.23e-12	>5e5	2.48e-07	8.48e-01	8.48e-01
Pu-238	9.74e-46	3.50e+03	1.92e-42	0.00	1.47e-35
Pu-239	1.82e-15	>5e5	2.10e-11	1.08e-07	2.23e-07
Pu240	2.96e-19	1.76e+05	2.86e-15	0.00	7.70e-17
Pu-242	1.61e-12	>5e5	6.75e-08	4.02e-01	4.02e-01
Am-241	2.04e-18	1.12e+04	2.91e-15	0.00	3.68e-15
Am-243	1.90e-12	1.06e+05	2.79e-07	0.00	7.37e-10

4 VARIATIONS

4.1 Diffusion upwards to the disturbed zone

There is a growing concern that the part of the rock adjacent to the excavated tunnels has a strongly increased permeability relative the surrounding rock (Pusch, 1990). This phenomenon is often called the disturbed zone. The disturbed zone may be a dominating path for the release of the radionuclides from a canister. In this section an analytic model for diffusion into a semi infinite buffer described in (Neretnieks, 1985) was used to investigate which of the nuclides can eliminated from further studies because they cannot pass through the bentonite barrier.

The method described in (Neretnieks, 1985) uses the so called H-parameter which is defined as:

$$H = z\left(\frac{\lambda}{D_a}\right)^{1/2} \tag{4-1}$$

z = transport distance in bentonite [m]
D_a = apparent diffusivity in bentonite [m^2/a]
l = decay constant [a^{-1}]

As was shown in the Finite Difference calculations the nuclides with a high solubility together with no or low sorption in the bentonite are not significantly retarded in the bentonite so the calculations below are mainly concerned with the solubility limited nuclides.
For these nuclides we have when $t \rightarrow \infty$:

$$C_{max} = C_{sol}e^{-H} \tag{4-2}$$

C_{max}= maximum concentration in buffer at distance z [mol]
C_{sol} = solubility concentration of nuclide [mol]

As can be seen in Equation (4-2) that for large H-values, C_{max}/C_{sol} becomes very small. For example with H = 15 we get $C_{max}/C_{sol} \approx 3 \cdot 10^{-7}$

The calculated values for H given in Table 4-1 were calculated for z = 0.35 m and z = 2 meter (the assumed as the transport distance upwards to the disturbed zone). The values used for the apparent diffusivities and solubility concentrations are the same as for the IFD calculations given in Tables 1-3 and 2-4.

The nuclides that have values underlined are those that would be eliminated if the criterion $H >$ 15 is used. That is, Ni-63, Pu-238, Pu-240, Am-241 and Sm-151 would be eliminated already for the 0.35 m case. For the 2 m case Am-243, Pu-239 would also be eliminated, with Pu-242 as a borderline case. As mentioned above this analytic model assumes a semi infinite medium for the bentonite which is not a conservative approach. On the other hand it does not include the large concentration drop outside the penetration hole in the canister which more than compensates for the semi infinite approximation.

Table 4-1
Maximum concentrations at 0.35 and 2 m distance into a semi infinite bentonite slab.

Nuclide	H (2 m)	H (0.35 m)	C_{max} (2 m)	C_{max} (0.35 m)
			[mol/m^3]	[mol/m^3]
Ni-59	3.4	0.6	3.42e-02	5.54e-01
Ni-63	93.1	16.3	<1.0e-30	8.41e-08
Se-79	0.3	0.1	7.49e-06	9.51e-06
Zr-93	1.5	0.3	6.56e-06	2.30e-05
Nb-94	4.2	0.7	1.55e-07	4.83e-06
Tc-99 red	5.8	1.0	6.15e-08	7.27e-06
Pd-107	0.1	~0.0	1.42e-03	1.49e-03
Sn-126	7.2	1.3	1.48e-08	5.66e-06
Ce-142	~0.0	~0.0	9.97e-06	9.99e-06
Sm-151	138.8	24.3	<1.0e-30	2.84e-16
Np-237	1.6	0.3	4.15e-07	1.52e-06
Pu-238	992.3	173.6	<1.0e-30	<1.0e-30
Pu-239	60.0	10.5	<1.0e-30	5.55e-10
Pu-240	114.9	20.1	<1.0e-30	3.69e-14
Pu-242	15.1	2.6	5.54e-12	1.42e-06
Am-241	109.7	19.2	<1.0e-30	2.76e-13
Am-243	26.6	4.6	1.75e-16	5.75e-07

4.2 Addition of film resistance at the bentonite/rock interface

In the preceding calculations has been assumed that the concentration in the fracture in the host rock is kept at zero and that there is no resistance for mass transfer from the bentonite to the water in the fracture. A few more IFD calculations have been made to exemplify the effect on the release rate of a film resistance between the bentonite and the water in the fracture. They have been made for Ni-59 and the film resistance values used are 1, 9 and 99 times the mass transfer resistance at steady state in the last cm of bentonite up to the fracture aperture as derived in Section 2.2.

Actually the boundary condition mass transfer coefficient α (which in the base case only represents the last cm of bentonite) has been decreased by a factor of 0.5, 0.1 and 0.01 keeping the boundary surface area the same. The release rates and integrated fraction released are shown together with the results for the base case in a separate diagram following the diagram for the base case for Ni-59 in Appendix A.

These particular values of film resistance could be translated into water flow velocity using the following assumptions:
- A single fracture is assumed to intersect the bentonite barrier. (A comment is made in Section 4.3 on the effect of the effect of several fractures intersecting the bentonite surface.)
- The fracture is plane with a uniform thickness of 0.5 mm. (Same as in the base case)
- The diffusivity in the free water is assumed to be $6 \cdot 10^{-2}$ m^2/year.
- The part of the bentonite perimeter which effectively interfaces with the flowing water (the contact angle) is assumed to be $\pi/4$ radians.

The film resistance is calculated by: (Nilsson et. al., 1991)

$$R_F = \sqrt{\frac{\Omega}{4\pi D_w u_f (r_2 + \sigma)\delta^2}} \qquad (4\text{-}3)$$

(The film resistance R_F is actually the inverse of the equivalent water flow rate.)

The release rates corresponding to the different film resistance values and the corresponding water velocities are shown in Table 4-2.

Table 4-2
Release rates for Ni-59 with a film resistance in the fracture.

R_F	u_f	Max release	Released fraction
[a/m]	[m^3/a]	[mol/a]	
0	-	$2.4 \cdot 10^{-6}$	$2.5 \cdot 10^{-1}$
437	$1.46 \cdot 10^{-2}$	$1.6 \cdot 10^{-6}$	$1.7 \cdot 10^{-1}$
3096	$1.80 \cdot 10^{-4}$	$4.1 \cdot 10^{-7}$	$5.2 \cdot 10^{-2}$
43103	$1.49 \cdot 10^{-6}$	$4.4 \cdot 10^{-8}$	$5.8 \cdot 10^{-3}$

4.3 Alternative diffusion geometries

The modelled scenario is one of several plausible combinations of holes in the canister wall and fractures intersecting the bentonite barrier. It is however thought to be representative for a number of other combinations as well.

As the non solubility limited nuclides because of no - or very small sorption all more or less quantitatively escape through the bentonite the following discussion is limited to the solubility limited nuclides.

There are three separate factors limiting the release rate.
- The bentonite thickness.
- The number and areas of holes in the canister wall.
- The number and aperture of fractures intersecting the bentonite barrier.

The bentonite thickness as such puts an upper limit on the instationary release rate for nuclides which have a half life much less than the time to penetrate that distance. This has already been discussed in Section 4.1 in terms of the *H*-parameter which actually is proportional to the square root of the ratio of penetration time to halflife. Penetration time is here loosely defined as the time it takes for the concentration at a certain distance into a slab of bentonite to rise to a specified fraction of the applied concentration on the surface. As was shown in Section 4.1 a number of the nuclides studied would not penetrate even the 0.35 m of bentonite to any appreciable extent just because of this. The effect of this limitation could be seen in the release curve for Nb-94 and Sn-126 for which the concentration reduction for the case described in Section 4.1 would be a factor 0.5 and 0.3 respectively. The release rate for Nb-94 has stabilised at a value of about 25% of the maximum possible taking the diffusion resistance near the hole into account as shown in Table 2-1. Sn-126 is still a factor of ten below the maximum calculated in Table 2-1 when the calculation is finished but is clearly approaching a steady state.

For most of the nuclides the area of the hole in the canister wall determines the release rates. As can be seen from Equation 2-4 the maximum release rate at steady state past a spherical shell with the area of the hole as inner surface is proportional to the diameter of the hole in the canister wall as long as it is small compared to the thickness of the bentonite barrier.

As the main concentration drop in the bentonite close the hole takes place over a distance of less than ten hole diameters the effect on nuclide release of adding several holes would be additive as long as they are more than that distance apart.

With the fracture and hole widths used the release of the solubility limited nuclides will be fairly insensitive to variations in the fracture aperture down to at least a tenth of the aperture value used.

The approximation made by restricting the modelled cross section area of the bentonite to 1 m^2 is minor because the dominating diffusion resistance near the hole would be unaffected by an addition of more bentonite after it. The effective length of the diffusion path from hole to fracture will remain constant. One possible side effect of including a wider sector of the bentonite would be to include a longer fracture aperture. This will though in most cases be counteracted by the larger amount of bentonite available for sorption with a proportionally lower concentration as result. Taking this into account the release rate would remain constant.

5 SUMMARY

The instationary diffusion of nuclides through the bentonite barrier surrounding a canister with spent nuclear fuel has been studied.

For the type of scenario chosen there are a small number of factors which determine the nuclide release whose values are measurable under laboratory conditions or possible to assess with some confidence. The scenario is in this respect quite robust.

The diffusion is assumed to take place between a small hole in the canister and the aperture of a fracture in the surrounding host rock. The converging diffusion paths to these area restrictions constitute a drastic limitation for the diffusive transport through the bentonite barrier. Particularly the limited area of the hole in the canister wall determines the release rates.

The other factor that determines the nuclide release is the solubility of the nuclide in question. No particular fuel dissolution model is credited for, just the solubility of the individual nuclides in the water filling voids inside the canister. Retention of nuclides in the canister because of limited rate of matrix dissolution is for instance not accounted for. At time zero all nuclides are available for dissolution. If the solubility can be correctly assessed for the exotic chemical environment inside the canister this assumption could be regarded as very conservative for many nuclides. All the non solubility limited nuclides studied have low retention in the bentonite and do more or less completely escape through the bentonite barrier.

A third factor is the rate by which nuclides penetrate an initially nuclide-free bentonite barrier. For a number of the studied nuclides this together with the half life is what ultimately would limit the maximum attainable release through 0.35 m of bentonite regardless of the geometry of the diffusion path. For a number of nuclides, particularly mainly of the trans uranium elements, the release rate is still increasing at the end of the calculation at $5 \cdot 10^5$ years.

6 NOTATION LIST

Variable	Meaning	Units
A	Area	m^2
a	Inner radius	m
b	Outer radius	m
$C,C_a,C_b,C(r)$	Nuclide concentration	mol/m^3
C_{eq}	See Section 2.4	mol/m^3
D_a	Apparent diffusivity	m^2/a
D_e	Effective diffusivity	m^2/a
D_w	Diffusivity in free water	m^2/a
H	See Equation 5-1	Dimensionless
K_d	Mass sorption coefficient	m^3/kg
l	Length of fracture aperture	m
N,N_{gap},N_0	Amount of nuclide	mol
$\dot{N}$	Release rate	mol/a
$Q_{eq},Q_{eq,\infty}$	Equivalent water flow rate	m^3/a
R_F	Film resistance in fracture	a/m^3
r	Radius	m
r_2	Outer radius of the bentonite barrier	m
t	Time	a
t_{leach}	Time a solid phase exists	a
u_f	Water flow velocity	m/a
z	Penetration depth	m

Greek letters		
α	Mass transfer coefficient	m/a
δ	Fracture aperture	m
ε_p	Effective diffusion porosity	Dimensionless
θ	Solid angle	Steradians
λ	Decay constant	a^{-1}
ρ_p	Bulk density	kg/m^3
σ	Penetration of bentonite into the fracture	m
ϕ	Angle	Radians

Subscripts		
0	Initial condition	
sol	(C_{sol}=solubility)	(mol/m^3)
gap	Canister void space	

7 REFERENCES

Brandberg, F. and K. Skagius, Porosity, Sorption and Diffusivity Data Compiled for the SKB 91 Study.
SKB Technical report 91-16, April 1991.

Carslaw, H.S. and J.C. Jaeger
Conduction of Heat in Solids, 2nd ed.
Oxford Univ Press, New York, 1959.

Edwards, A. L., TRUMP: A Computer Program for Transient and Steady State Temperature Distributions in Multidimensional Systems, report, Natl. Tech. Inf. Serv., Nat. Bur. of Standards, Springfield, VA., 1969.

Neretnieks, I., Diffusivities of Some Constituents in Compacted Wet Bentonite Clay and the Impact on Radionuclide Migration in the Buffer. Nuclear Technology (71), 458–470, 1985.

Nilsson, L., L. Moreno, I. Neretnieks and L. Romero.
A Resistance Network Model Describing the Transport of Radionuclides int the Near Field Surrounding a Surrounding a Repository for Nuclear Waste.
SKB Technical Report, 1991, in preparation.

Pusch, R., Radionuclide Transport Paths in the Near Field — A KBS-3 Study. SKB Technical Report 90-32, 1990.

Appendix A

Diagrams with

Release rate and released fraction.

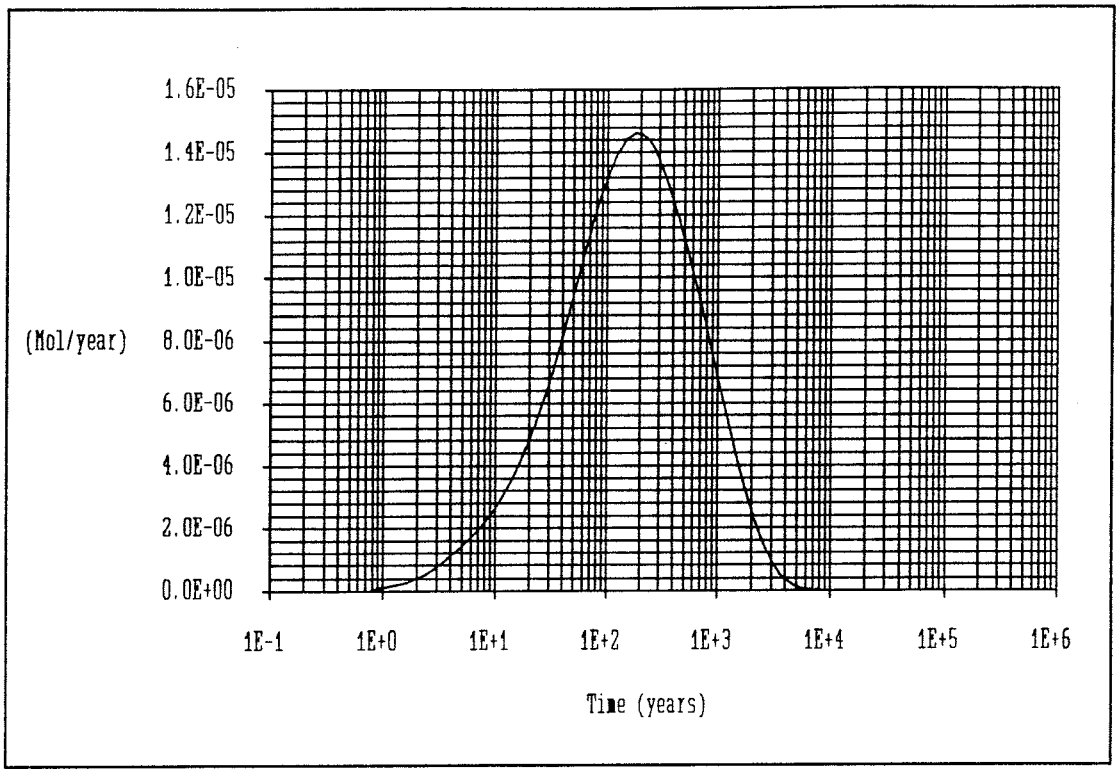

Figure 1
Release rate

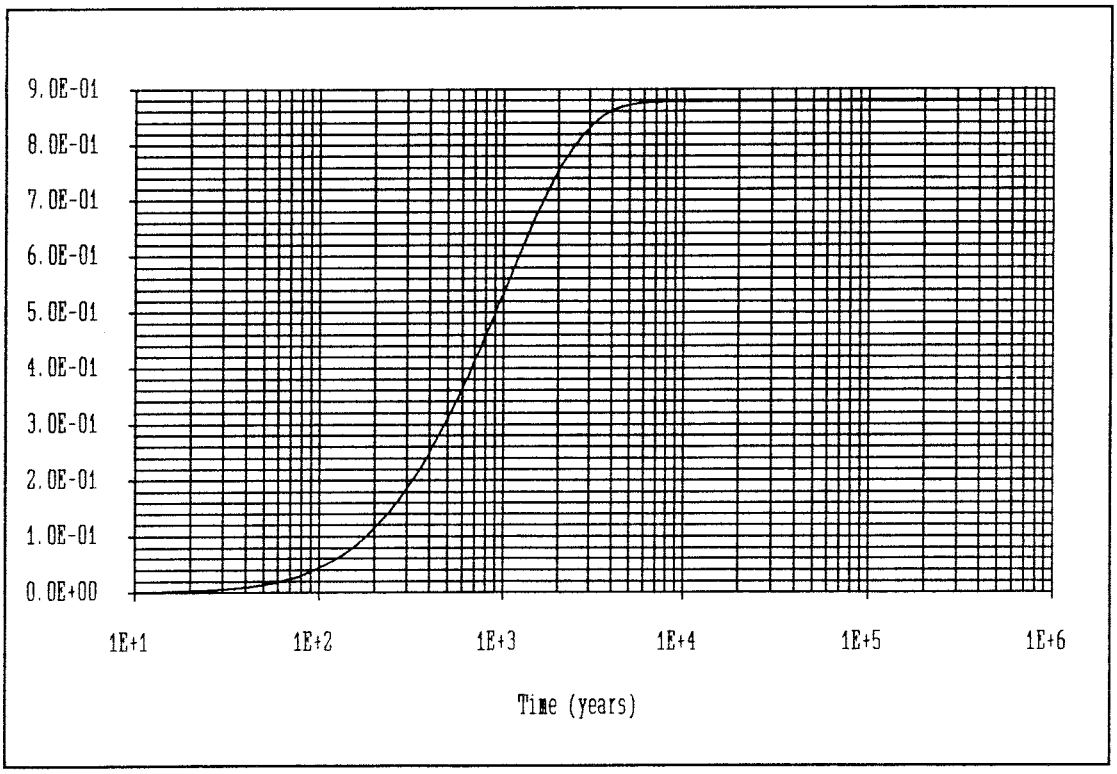

Figure 2
Released fraction.

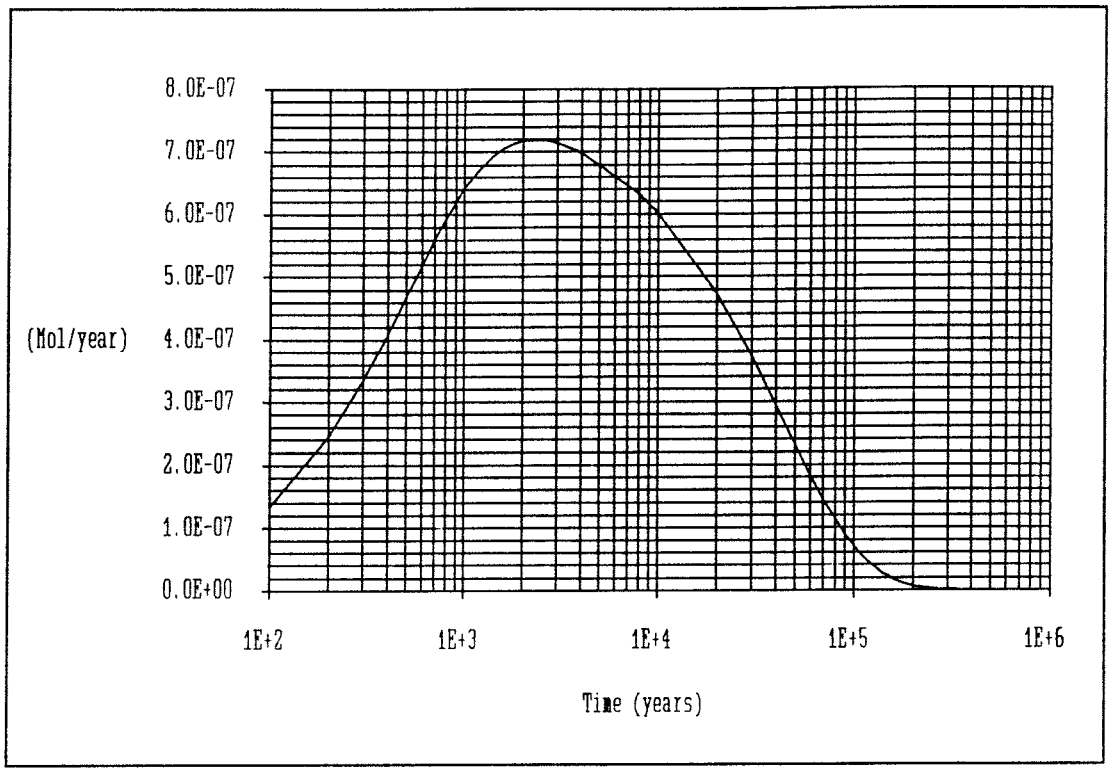

Figure 3
Release rate

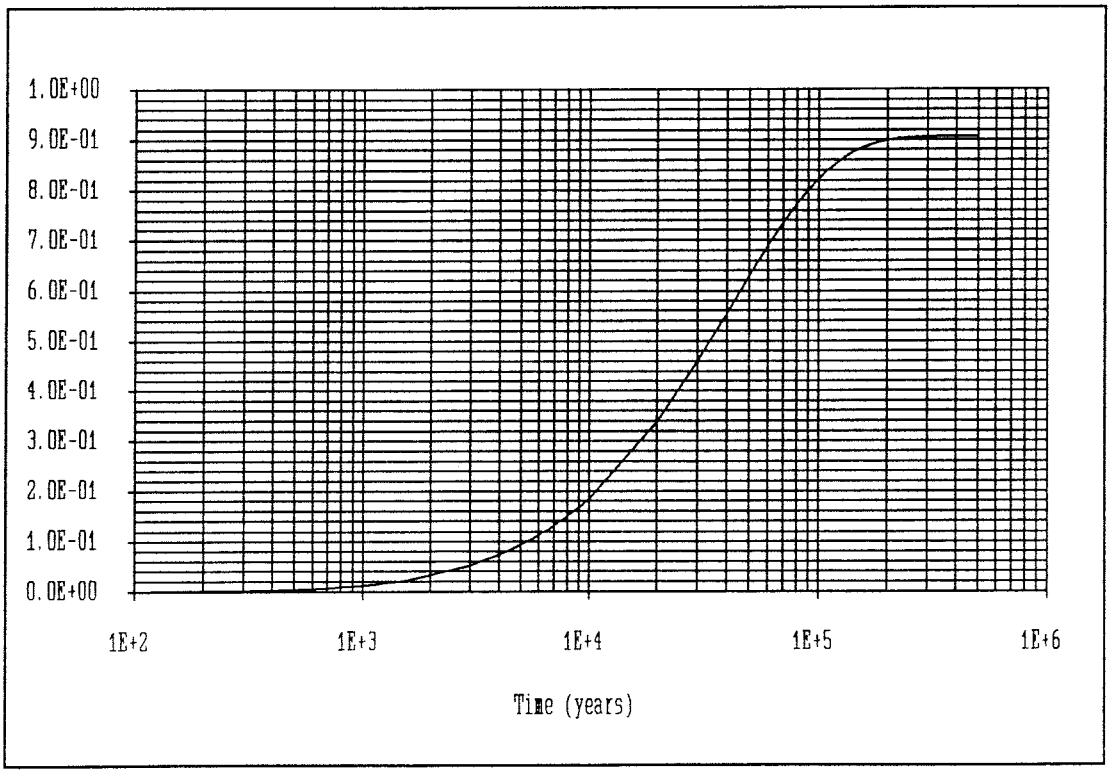

Figure 4
Released fraction.

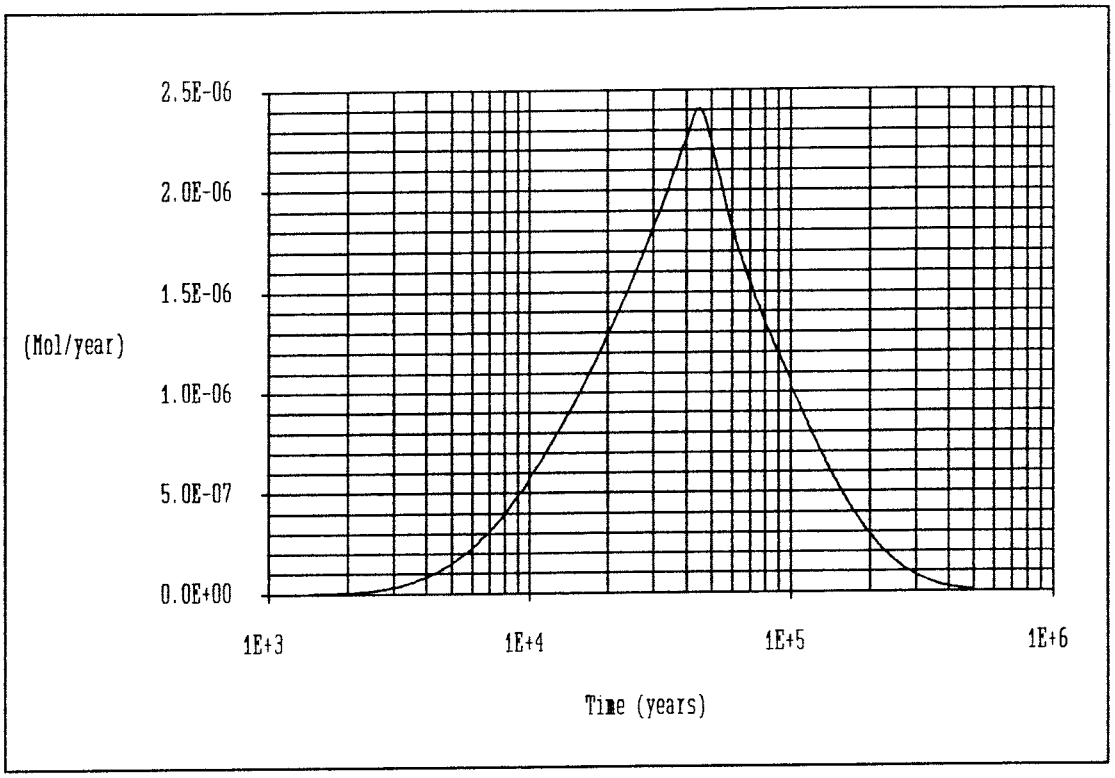

Figure 5
Release rate

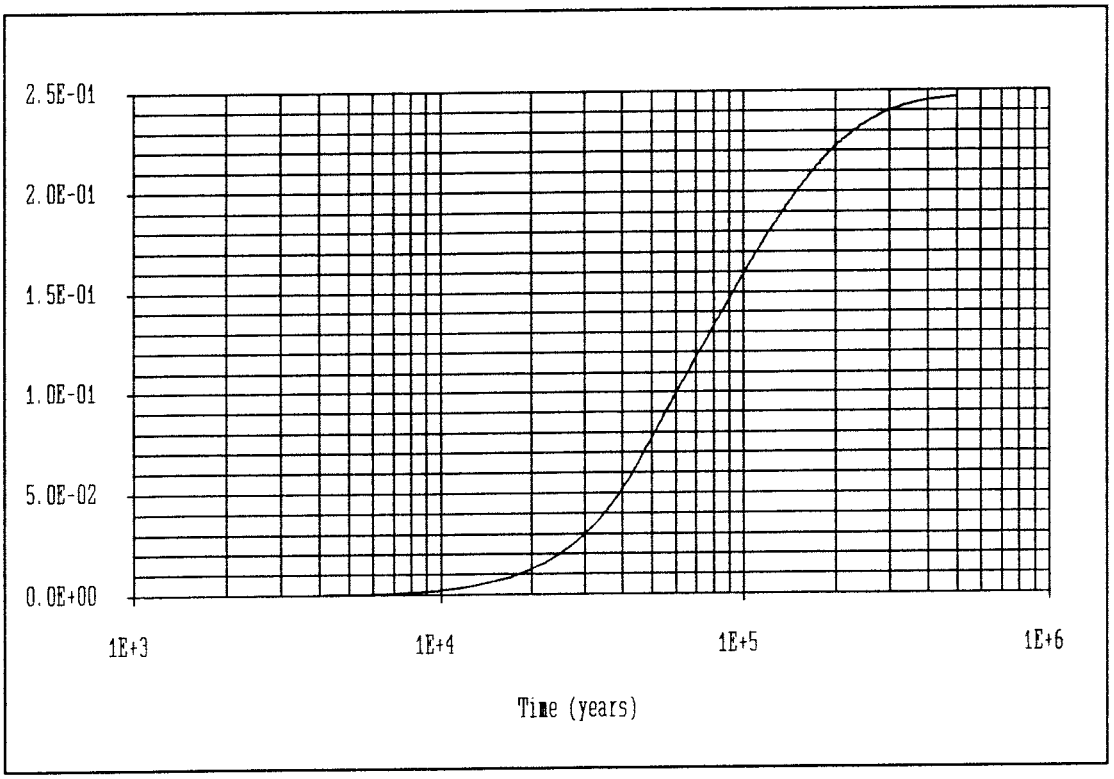

Figure 6
Released fraction.

Ni-59, film resistance in fracture added.

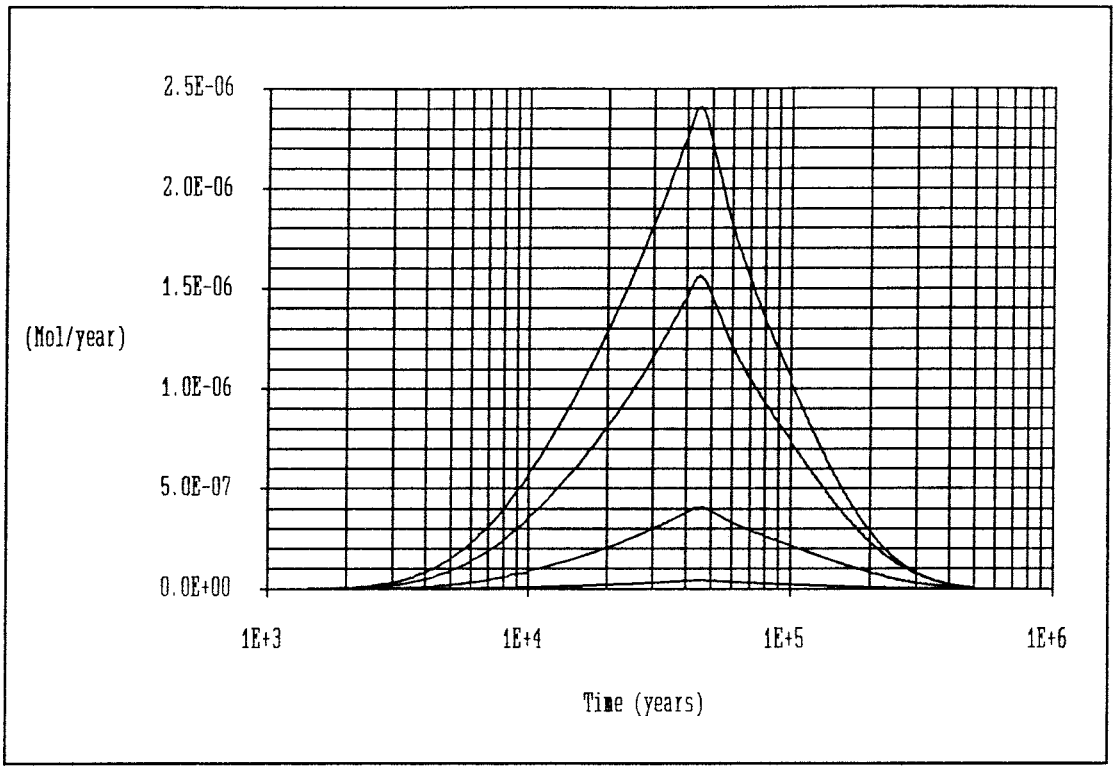

Figure 7
Release rate

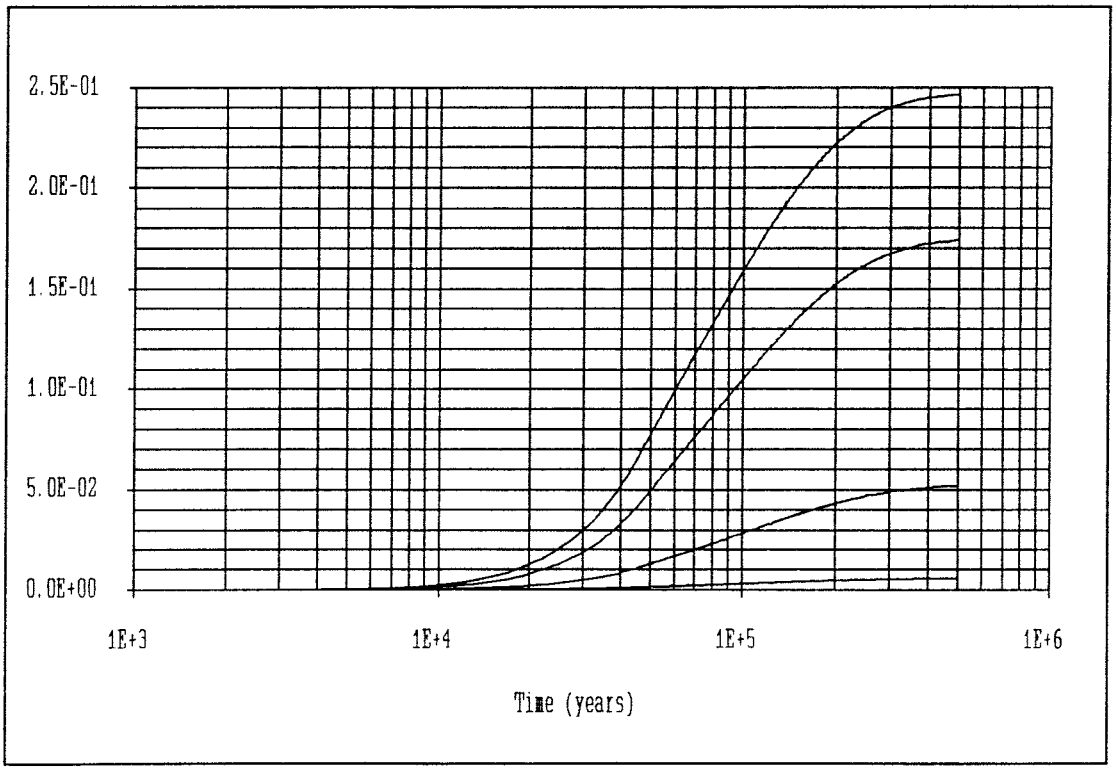

Figure 8
Released fraction.

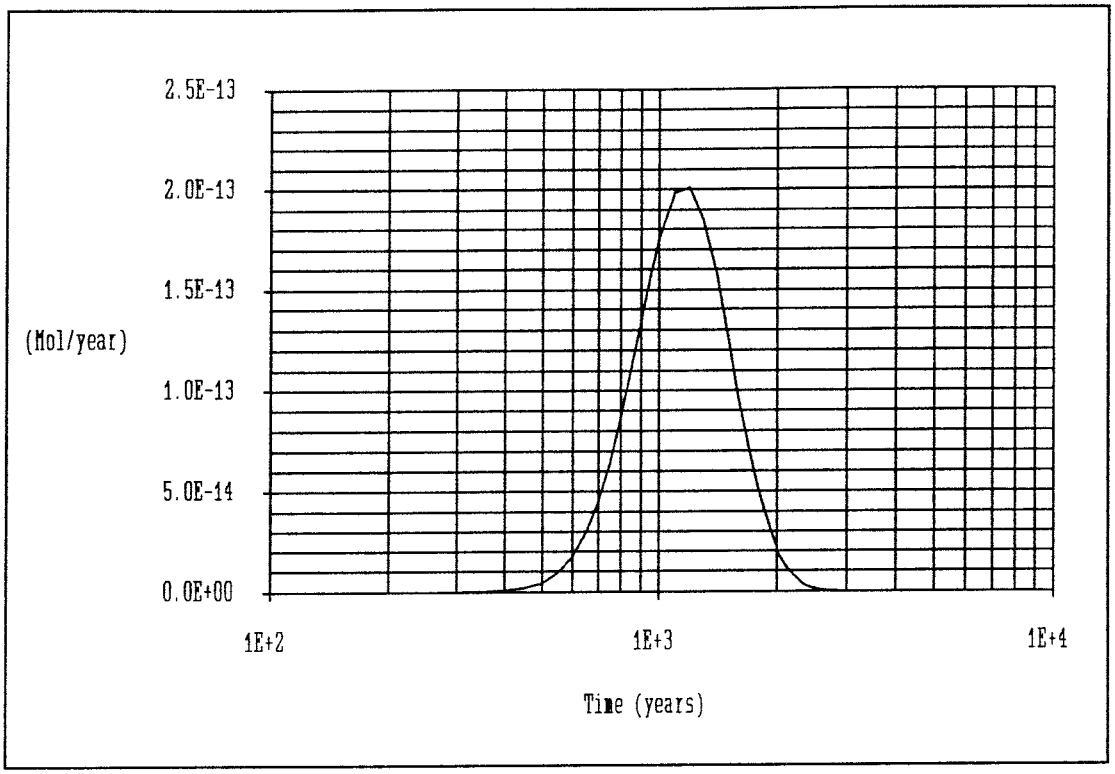

Figure 9
Release rate

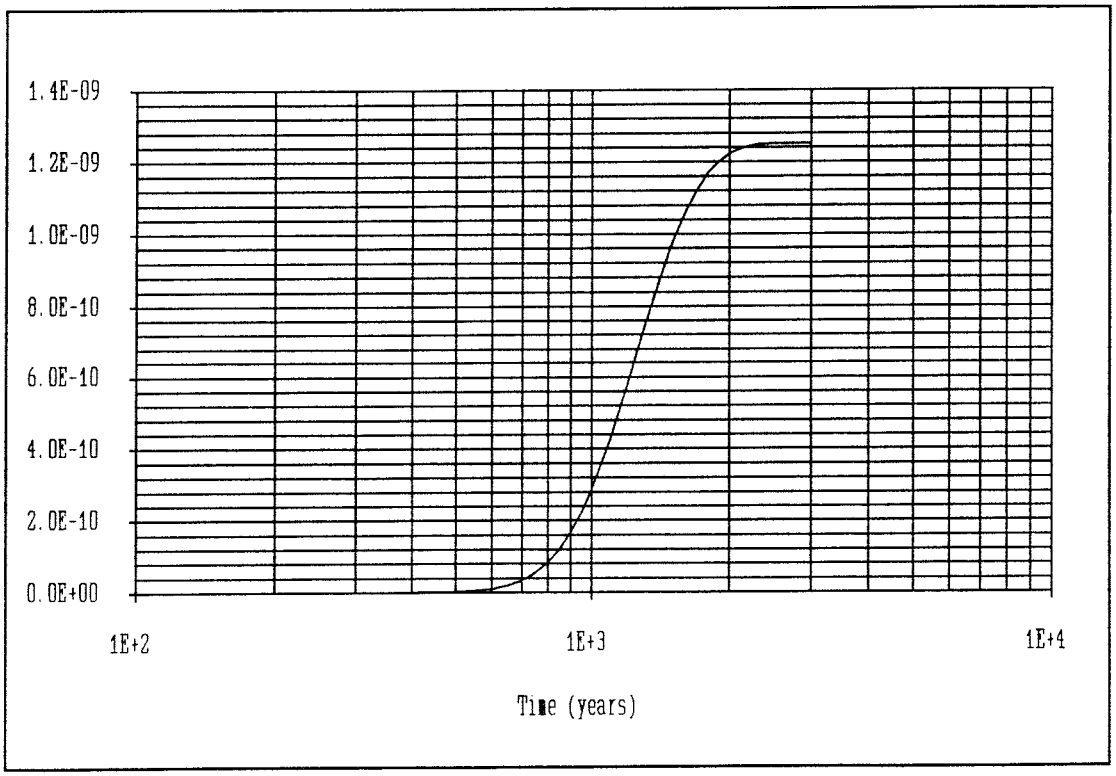

Figure 10
Released fraction.

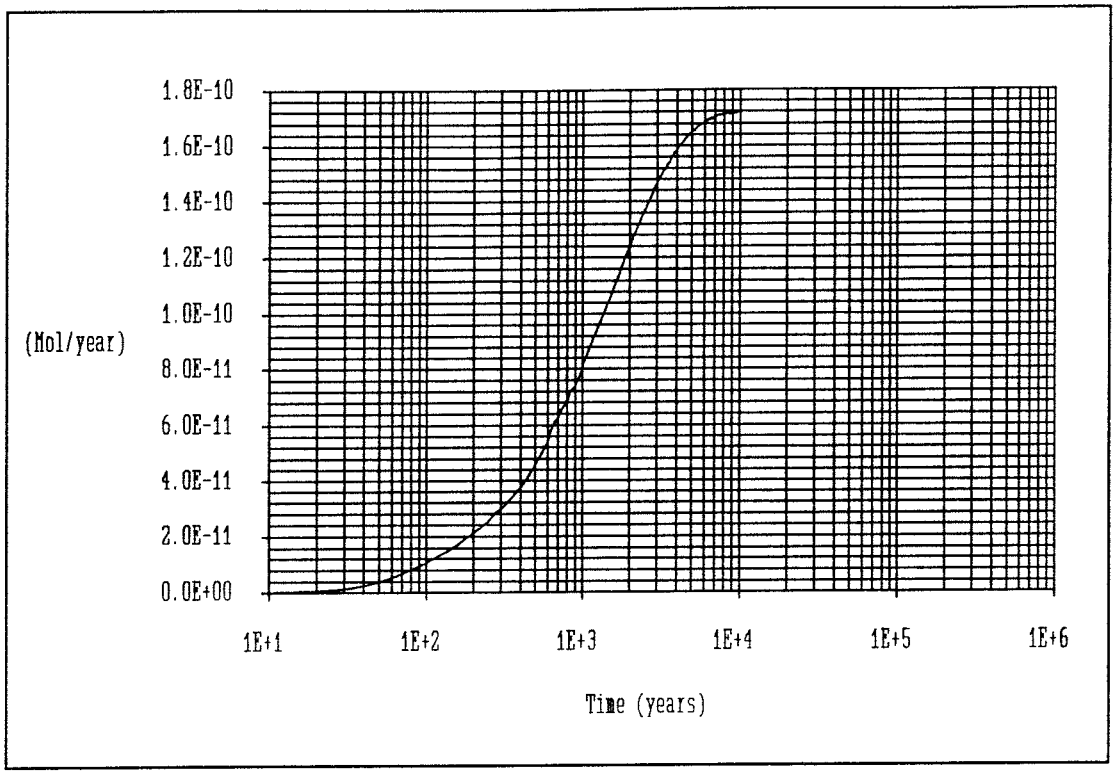

Figure 11
Release rate

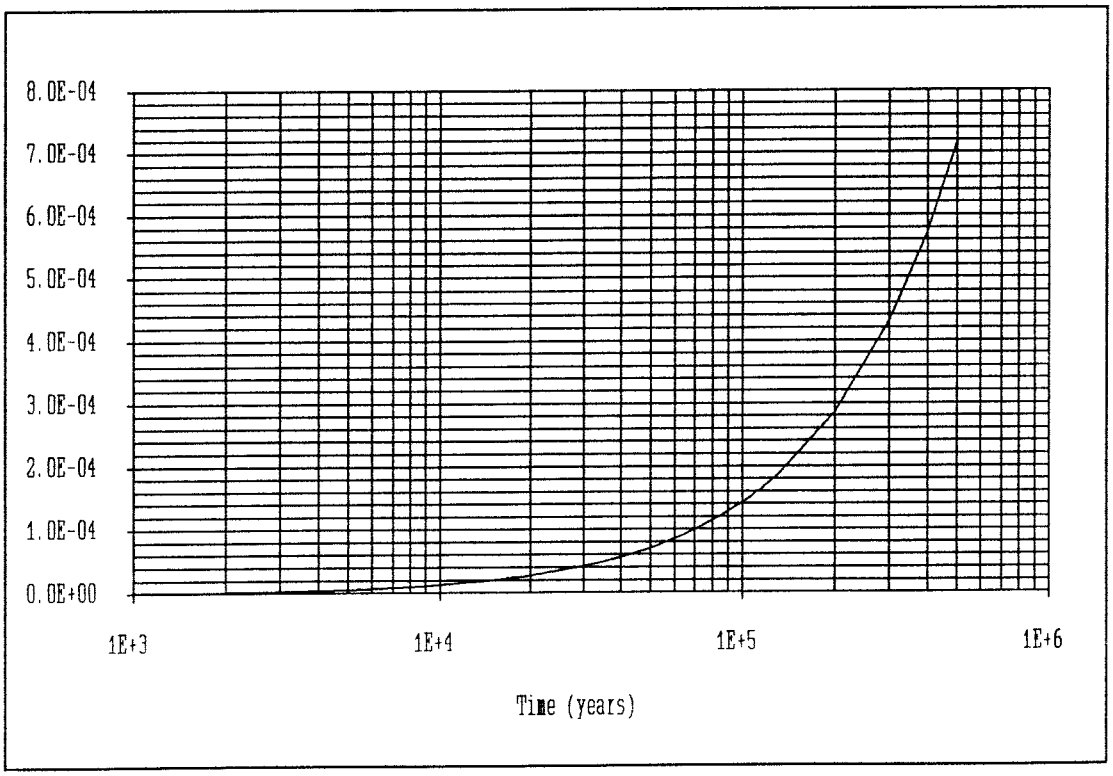

Figure 12
Released fraction.

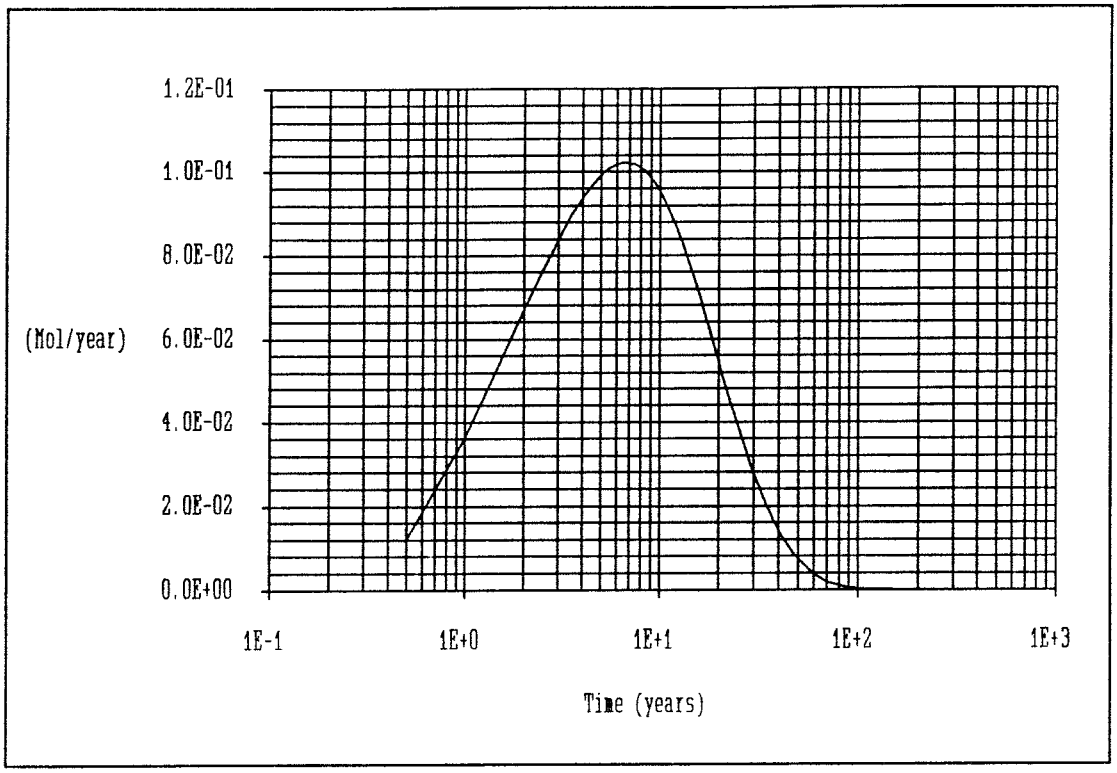

Figure 13
Release rate

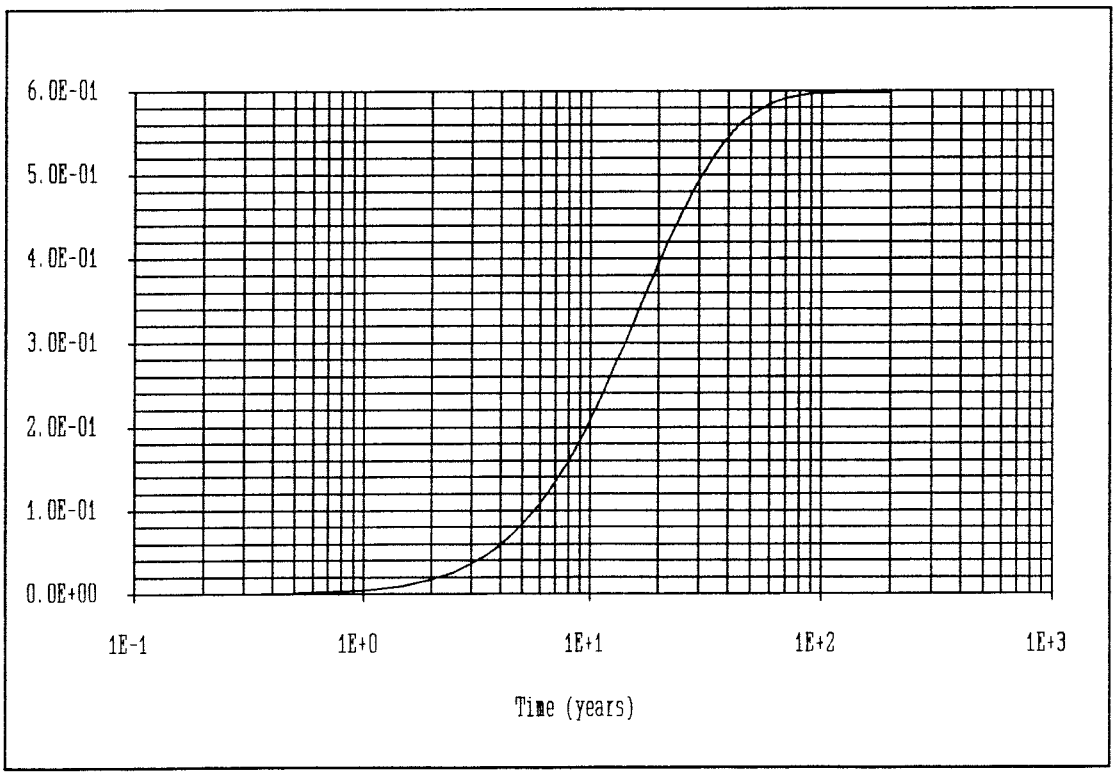

Figure 14
Released fraction.

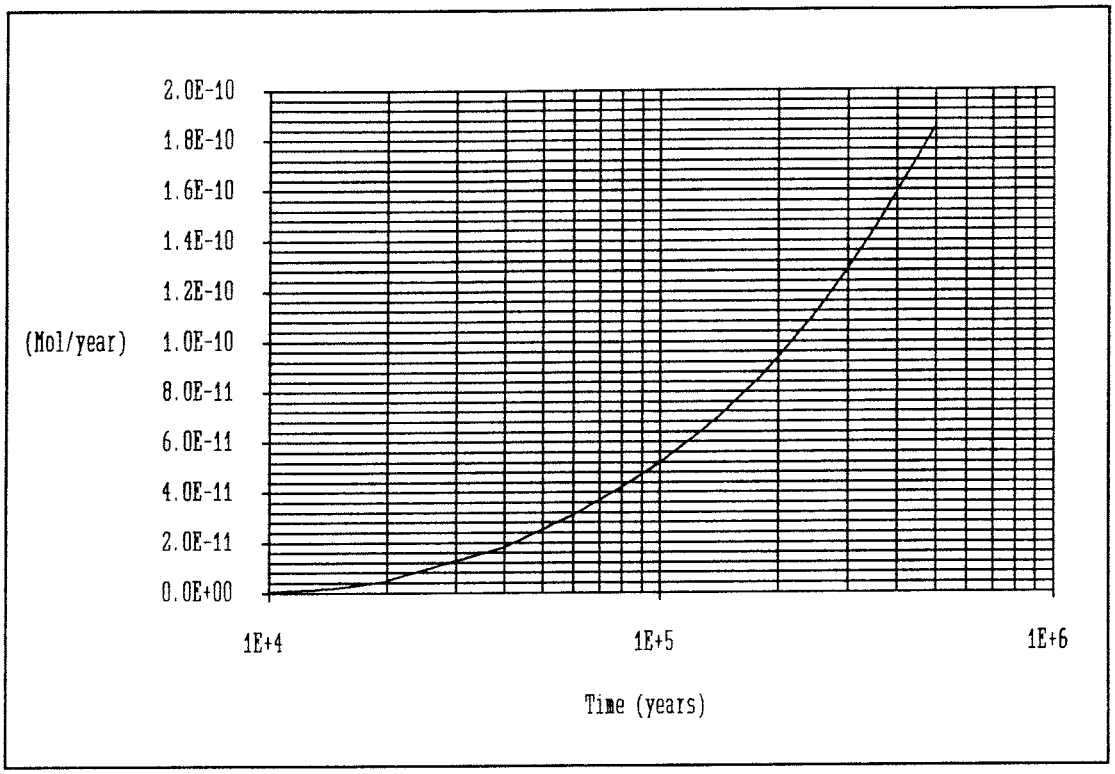

Figure 15
Release rate

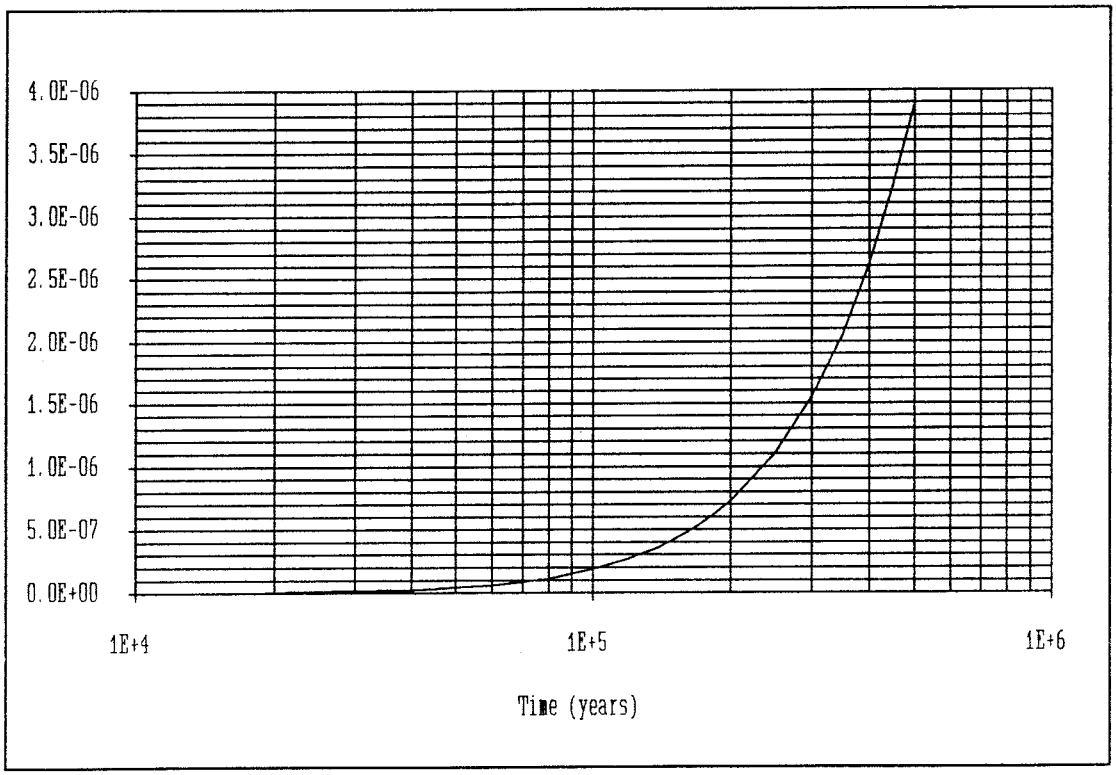

Figure 16
Released fraction.

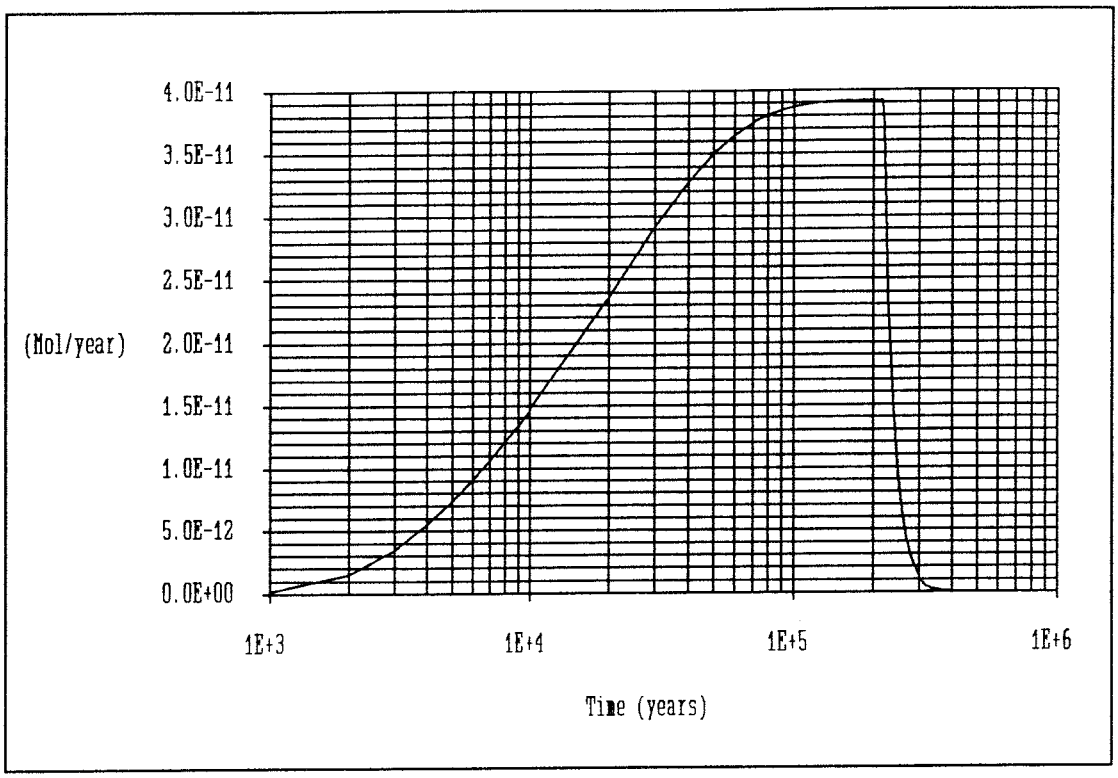

Figure 17
Release rate

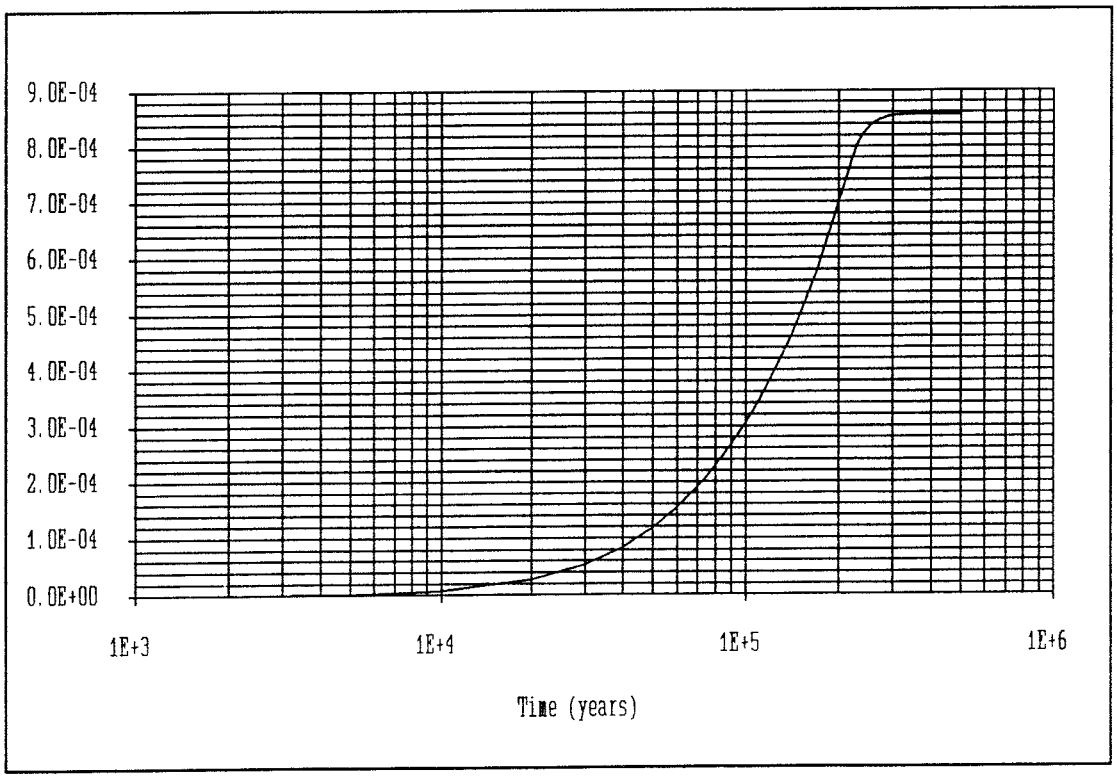

Figure 18
Released fraction.

Tc-99, Oxidising environment.

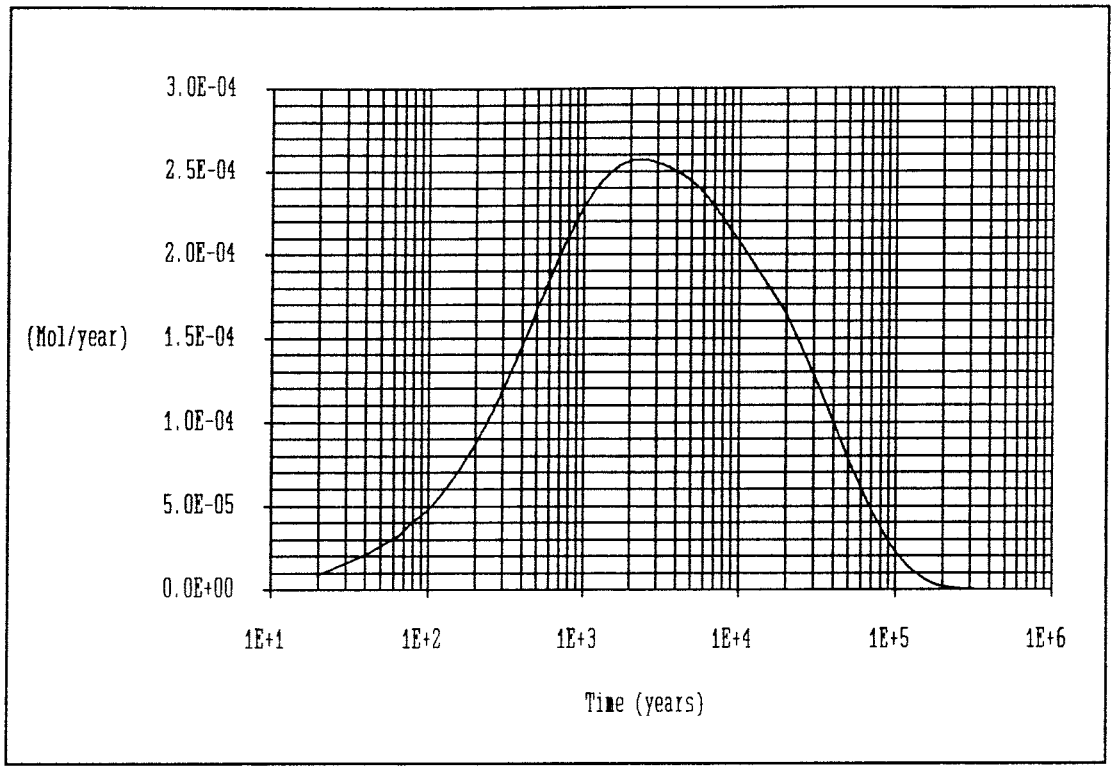

Figure 19
Release rate

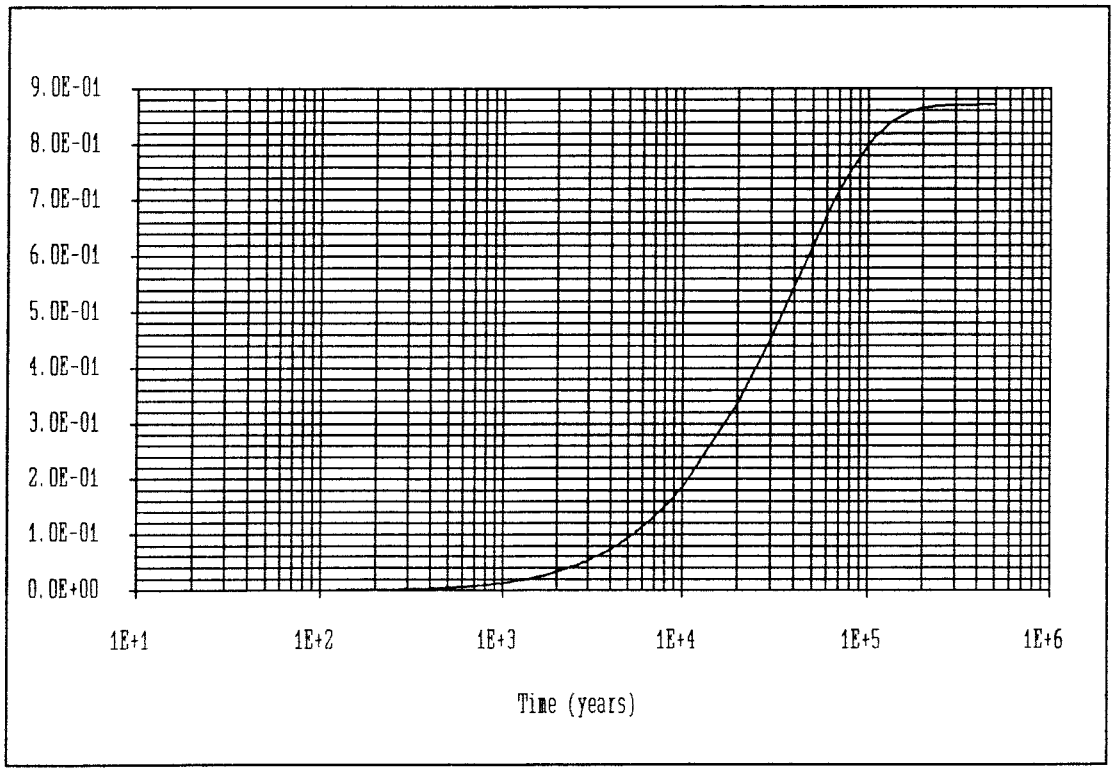

Figure 20
Released fraction.

Tc-99, Reducing environment.

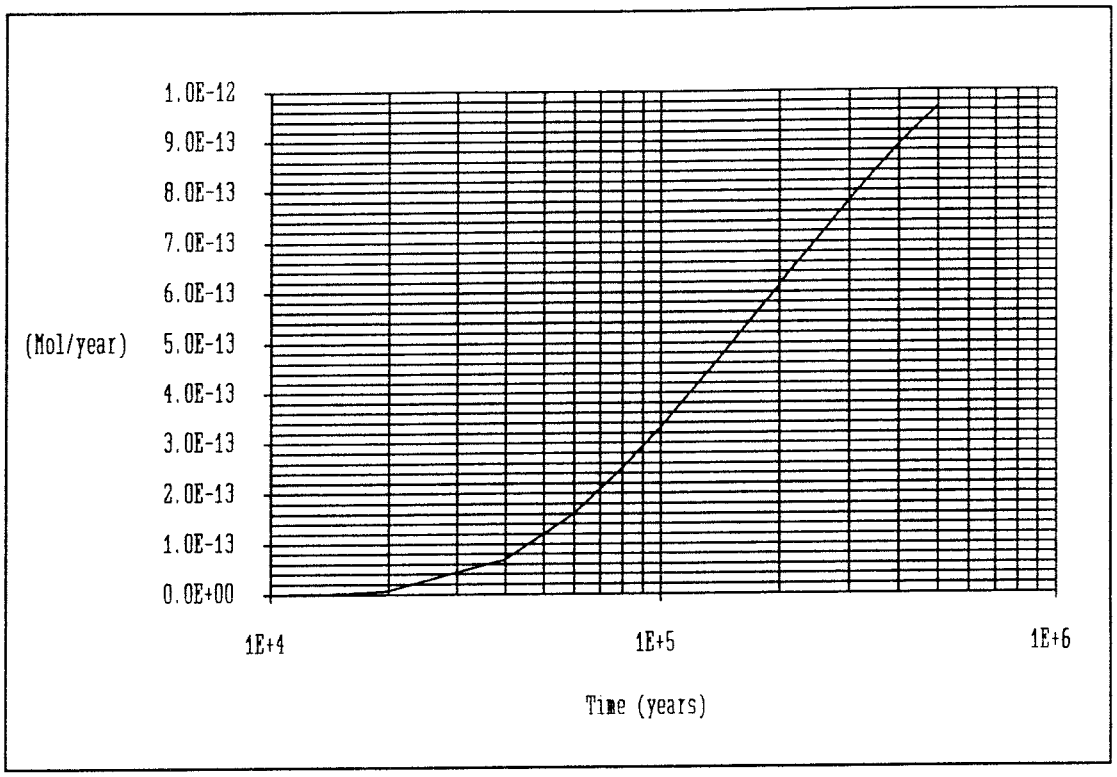

Figure 21
Release rate

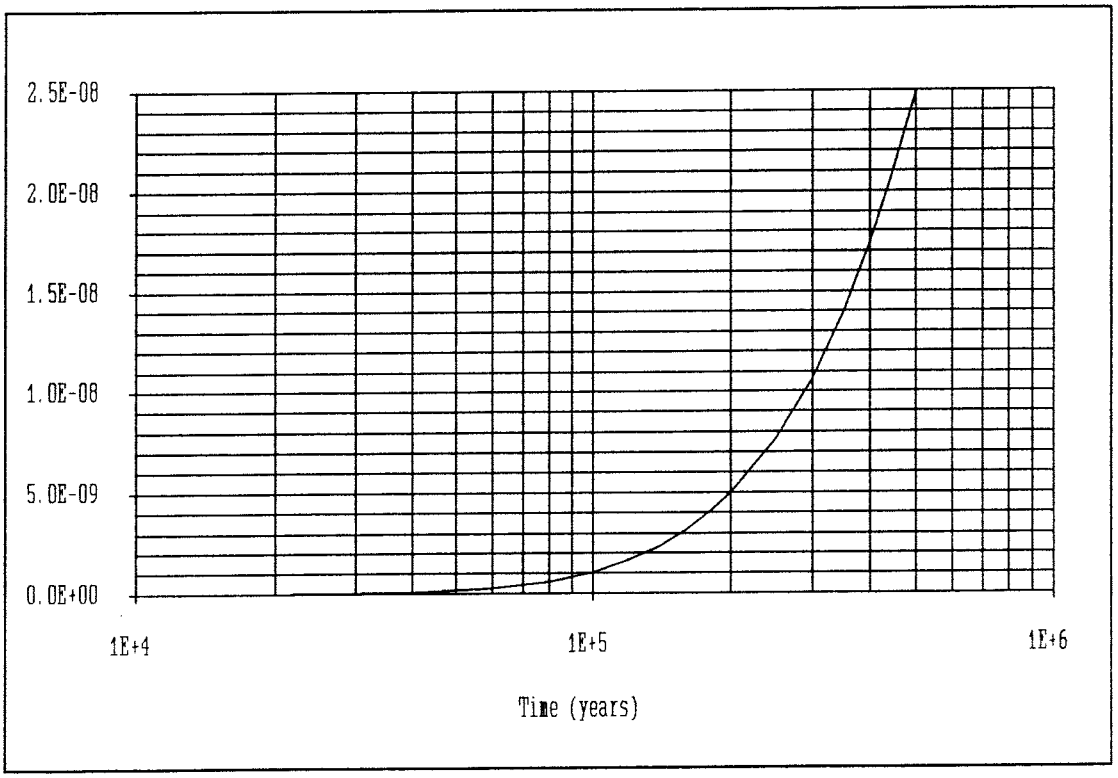

Figure 22
Released fraction.

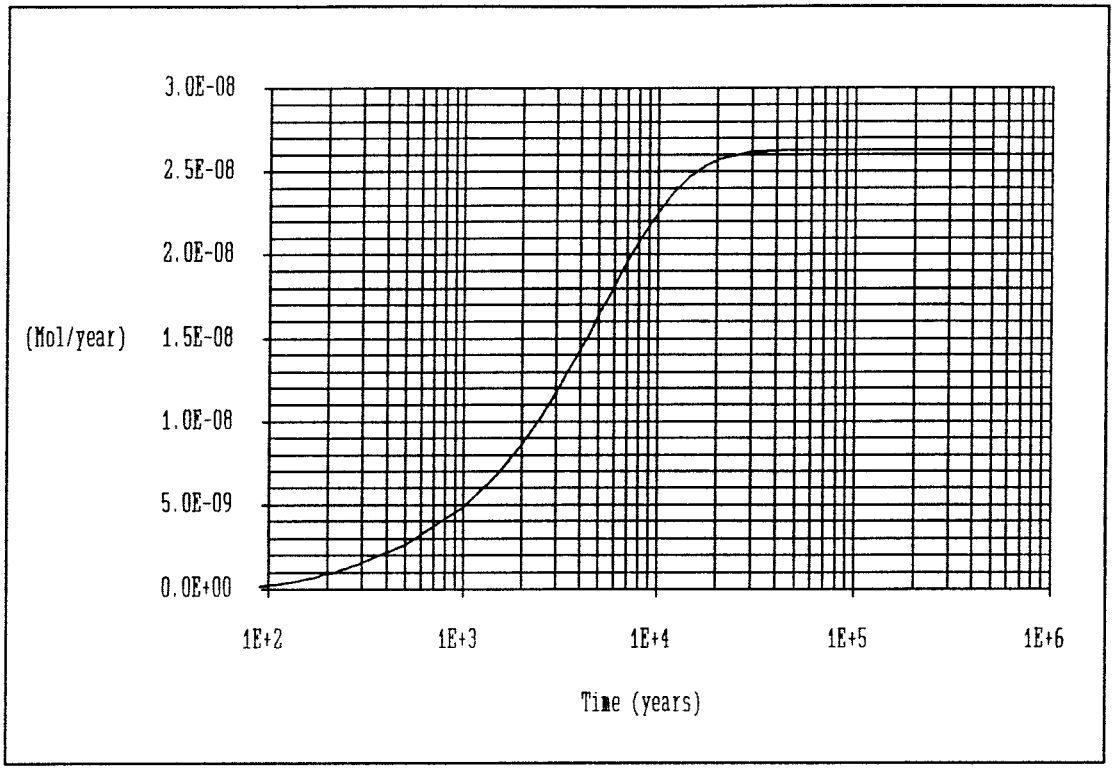

Figure 23
Release rate

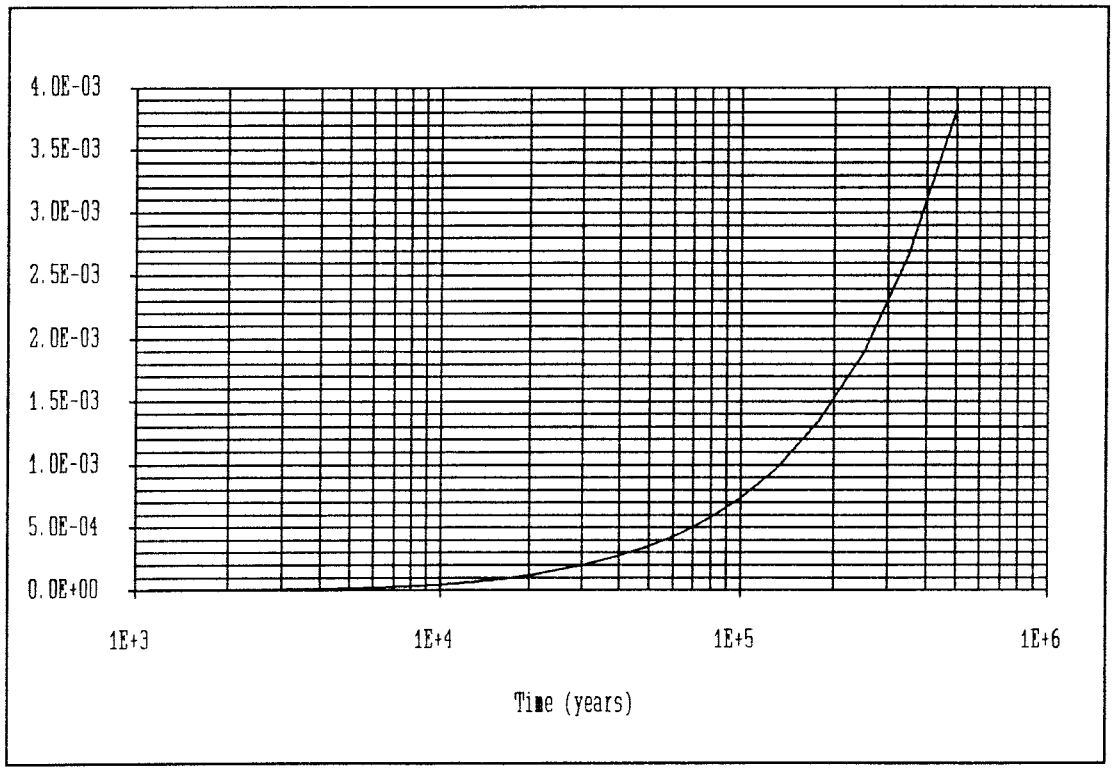

Figure 24
Released fraction.

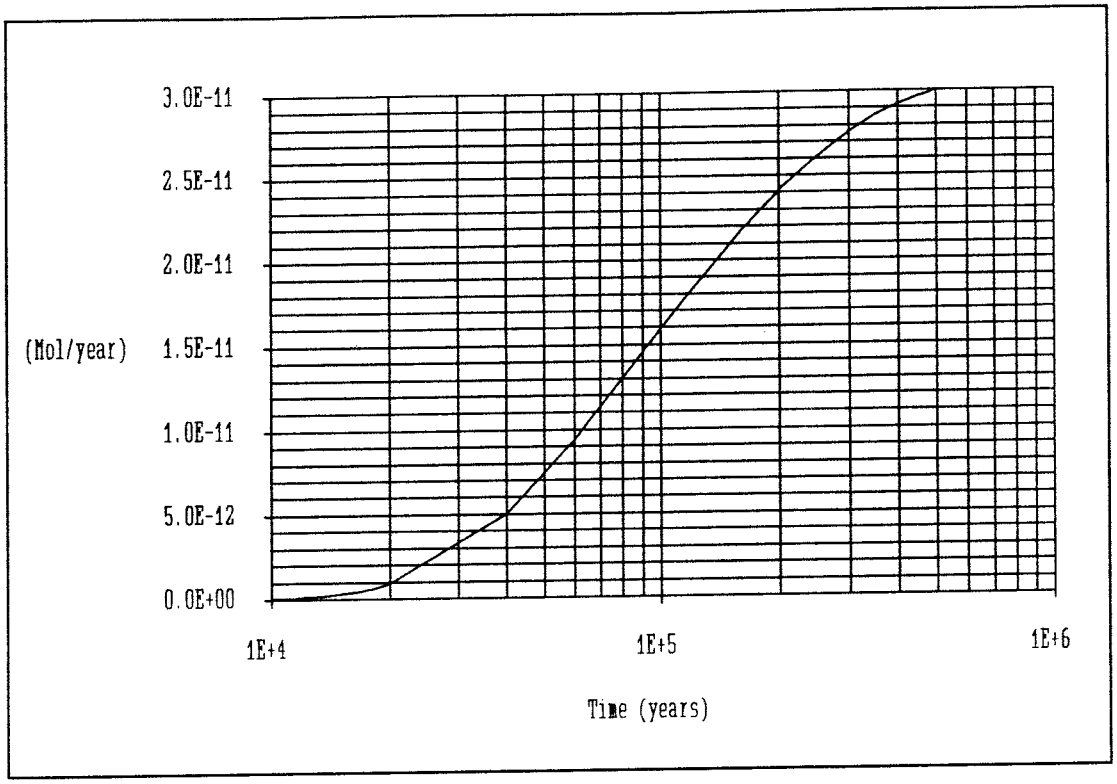

Figure 25
Release rate

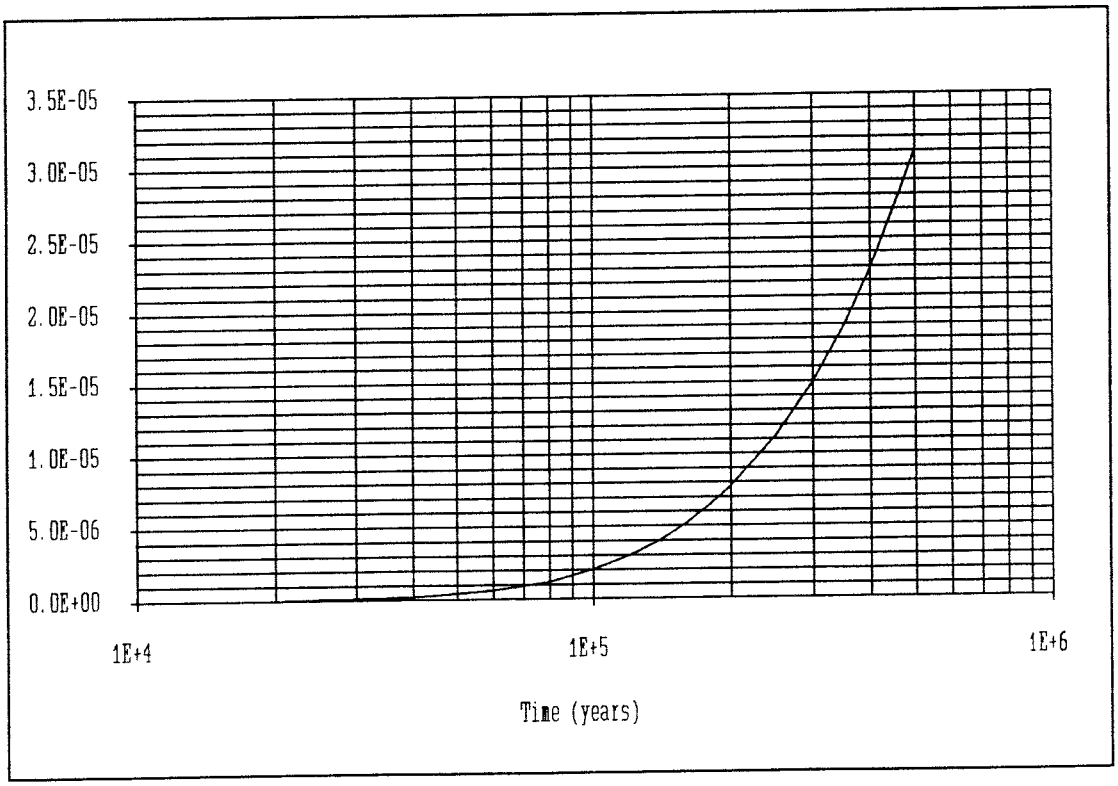

Figure 26
Released fraction.

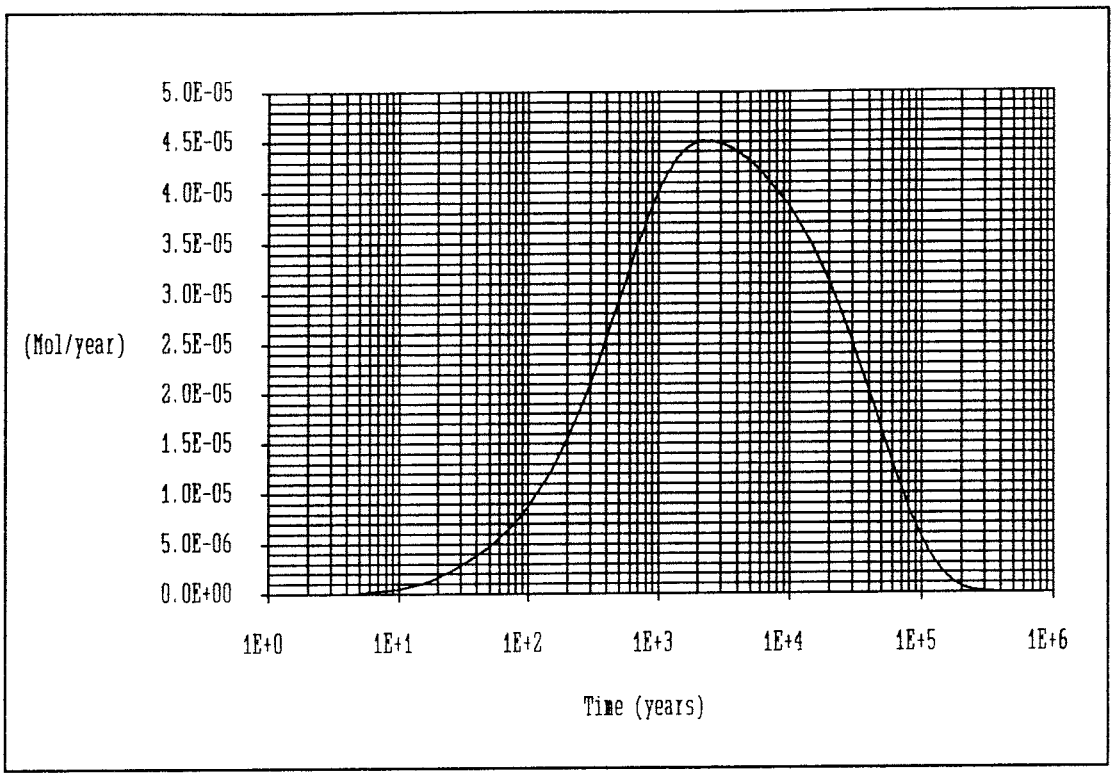

Figure 27
Release rate

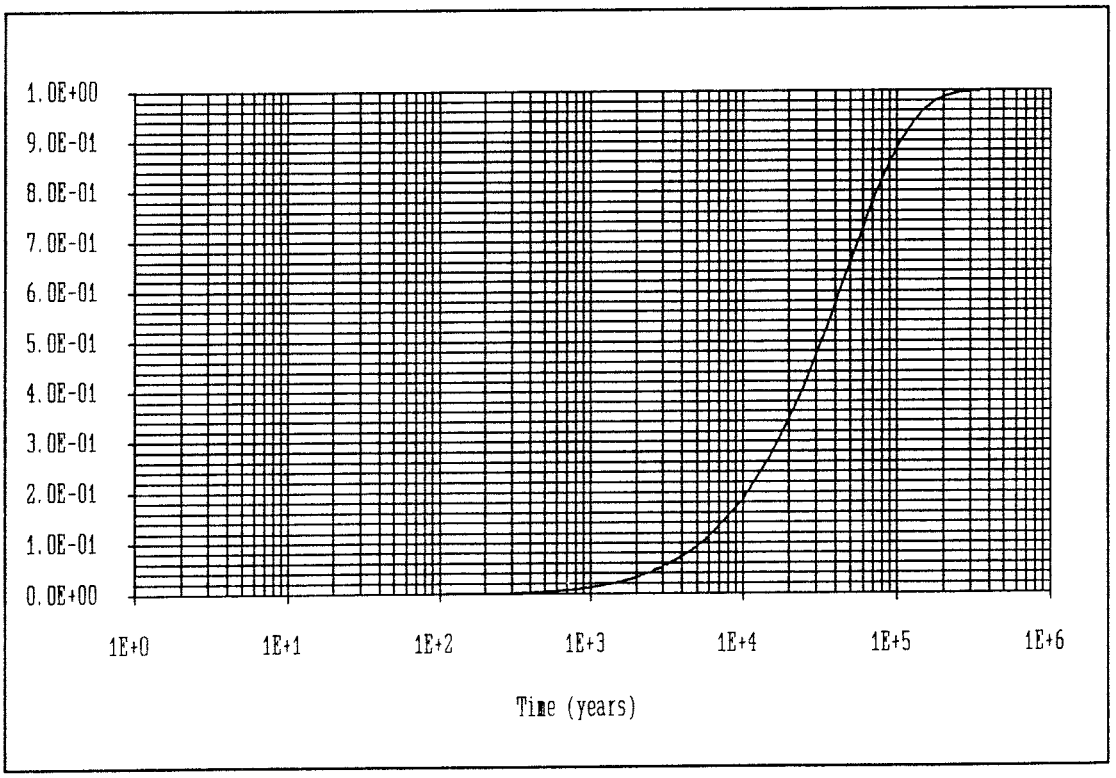

Figure 28
Released fraction.

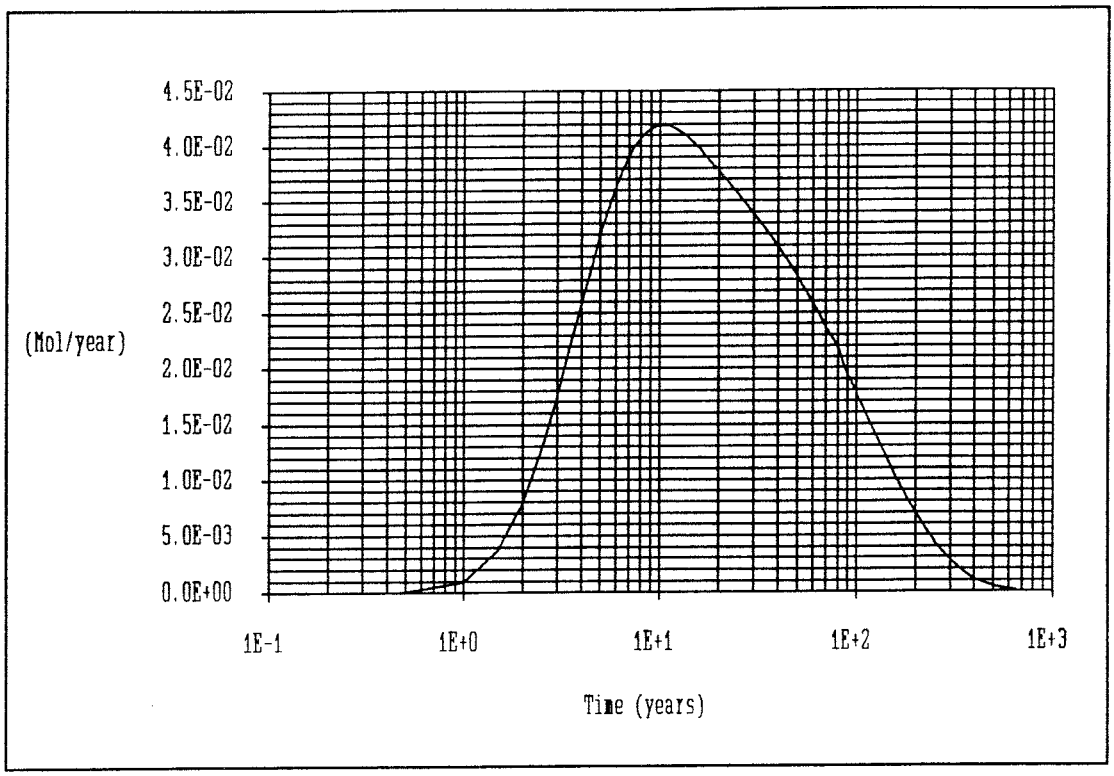

Figure 29
Release rate

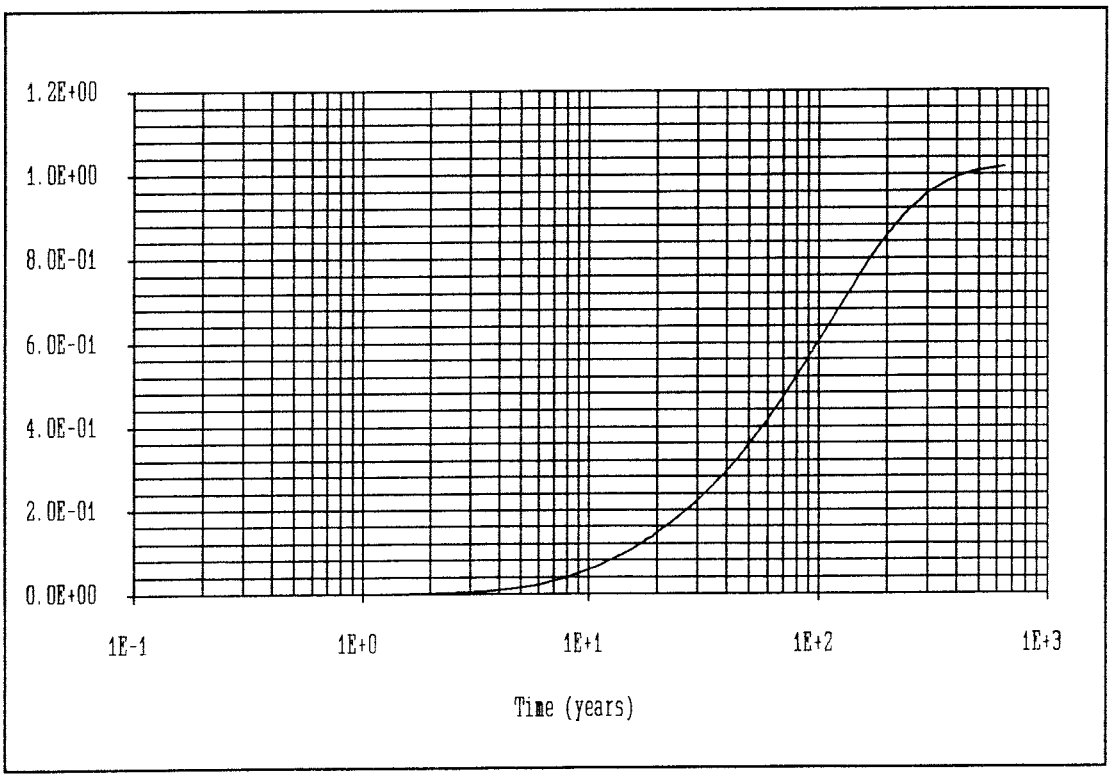

Figure 30
Released fraction.

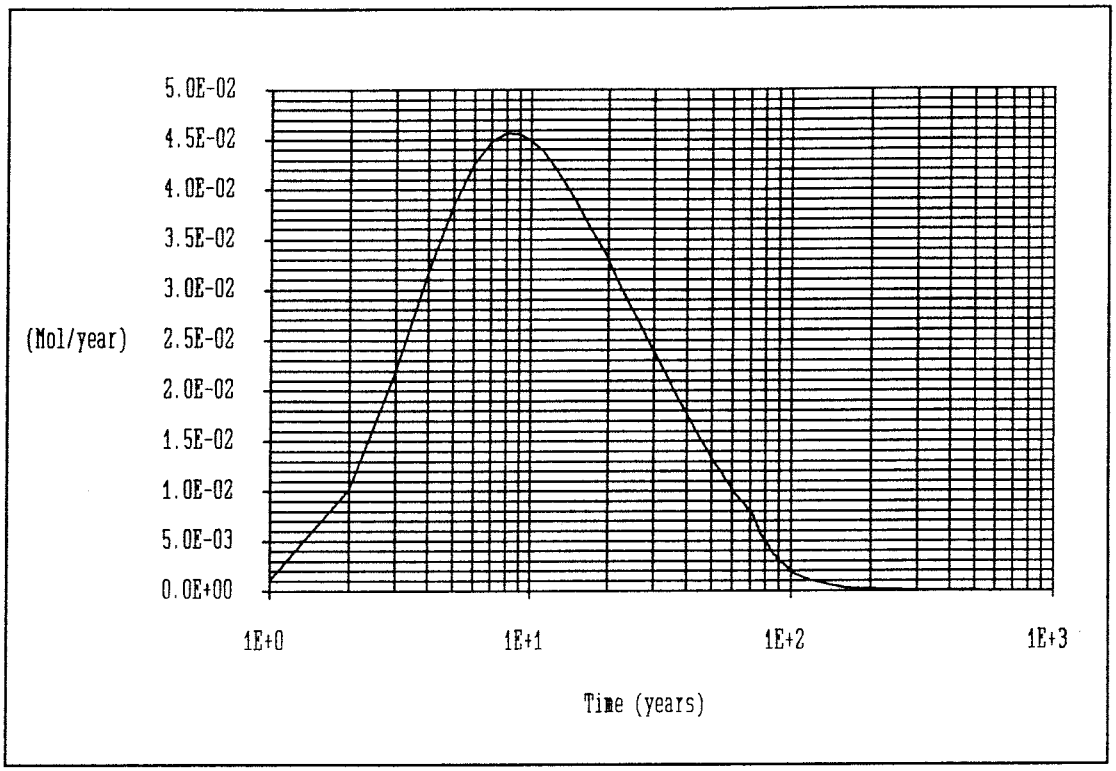

Figure 31
Release rate

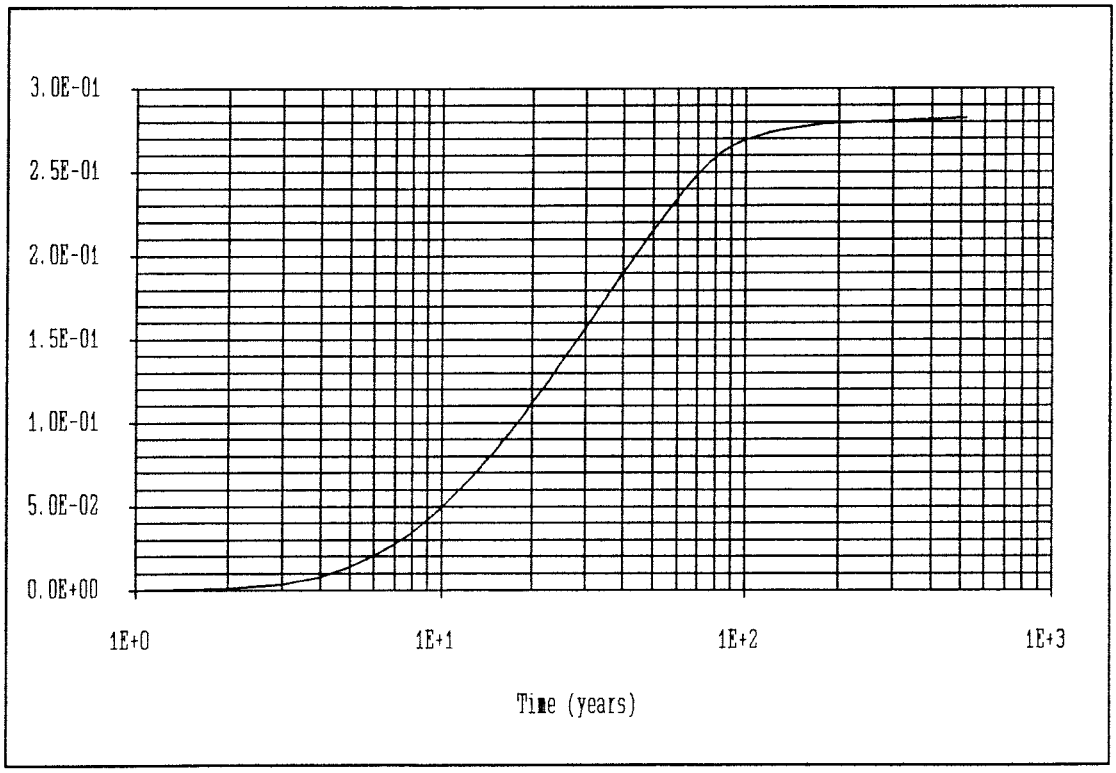

Figure 32
Released fraction.

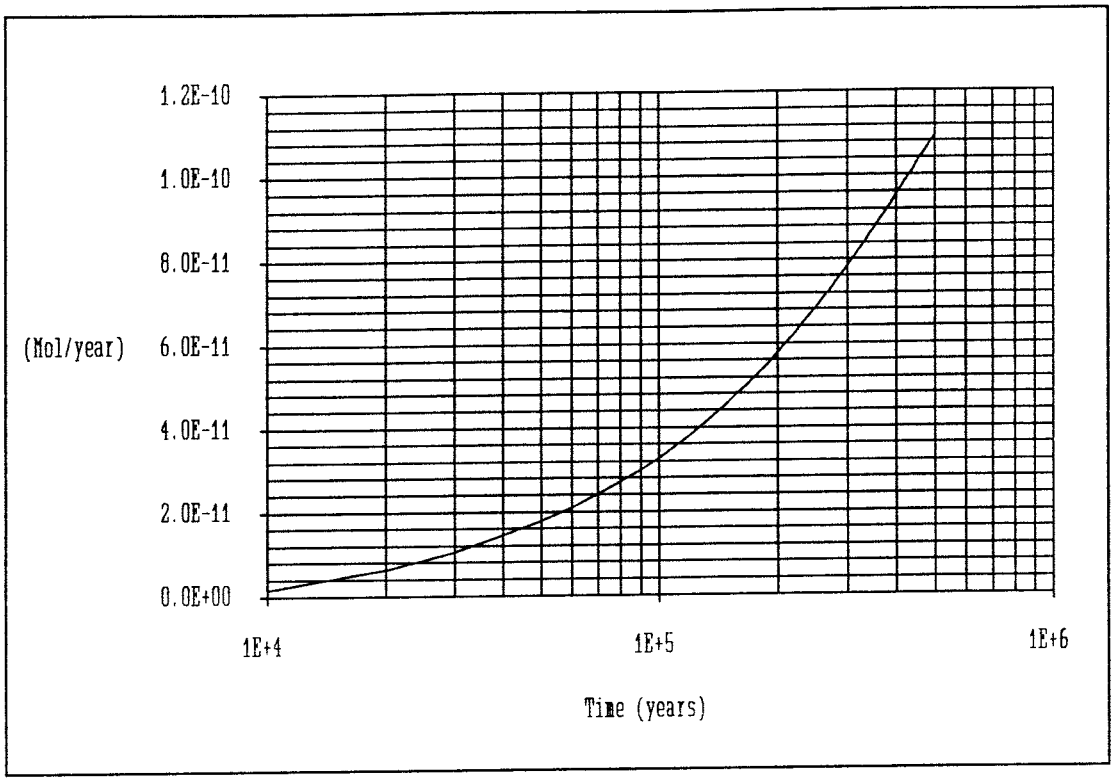

Figure 33
Release rate

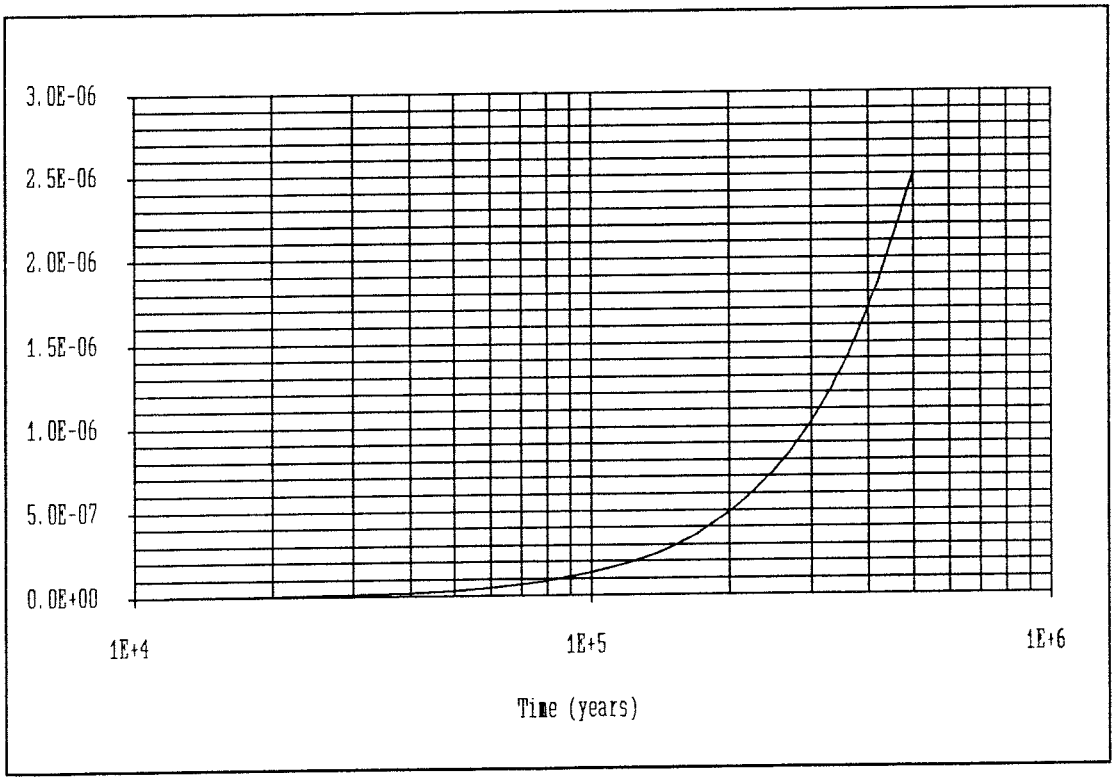

Figure 34
Released fraction.

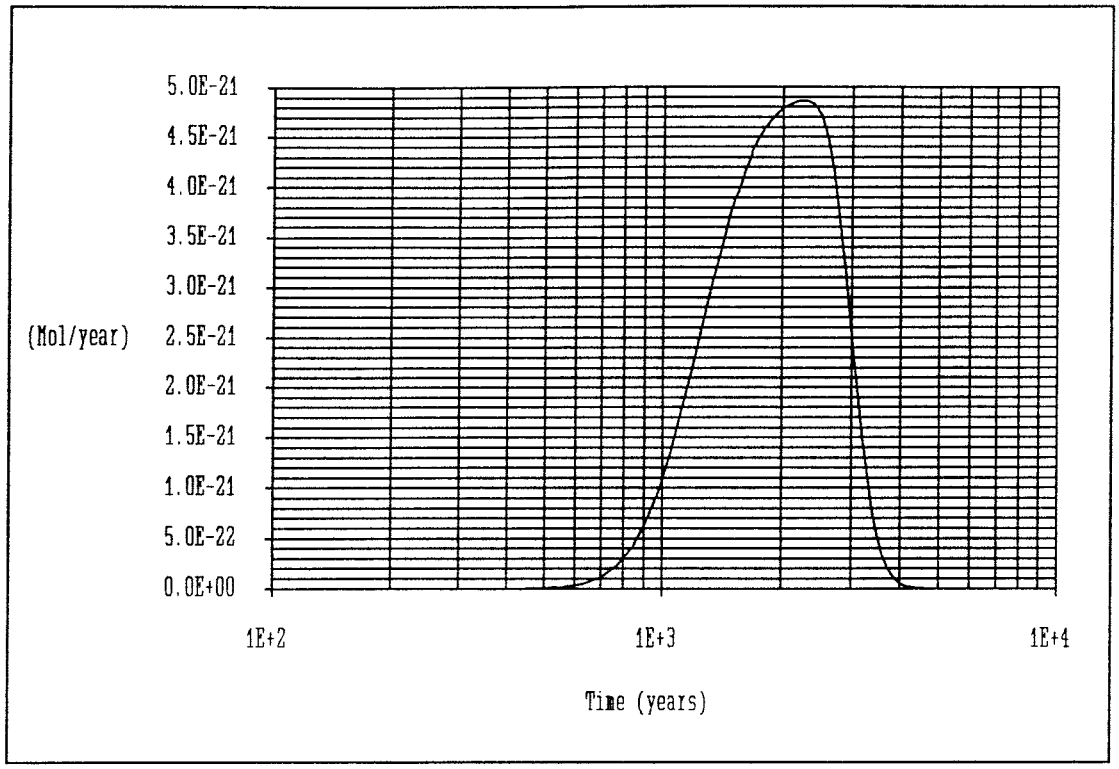

Figure 35
Release rate

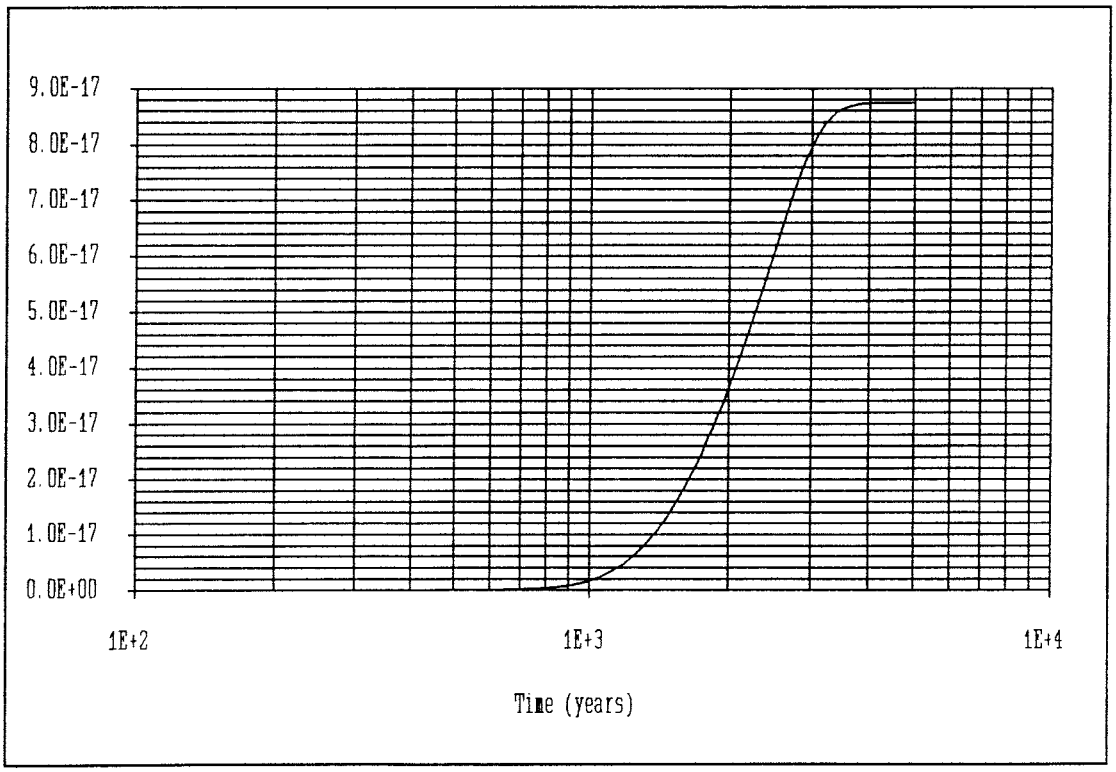

Figure 36
Released fraction.

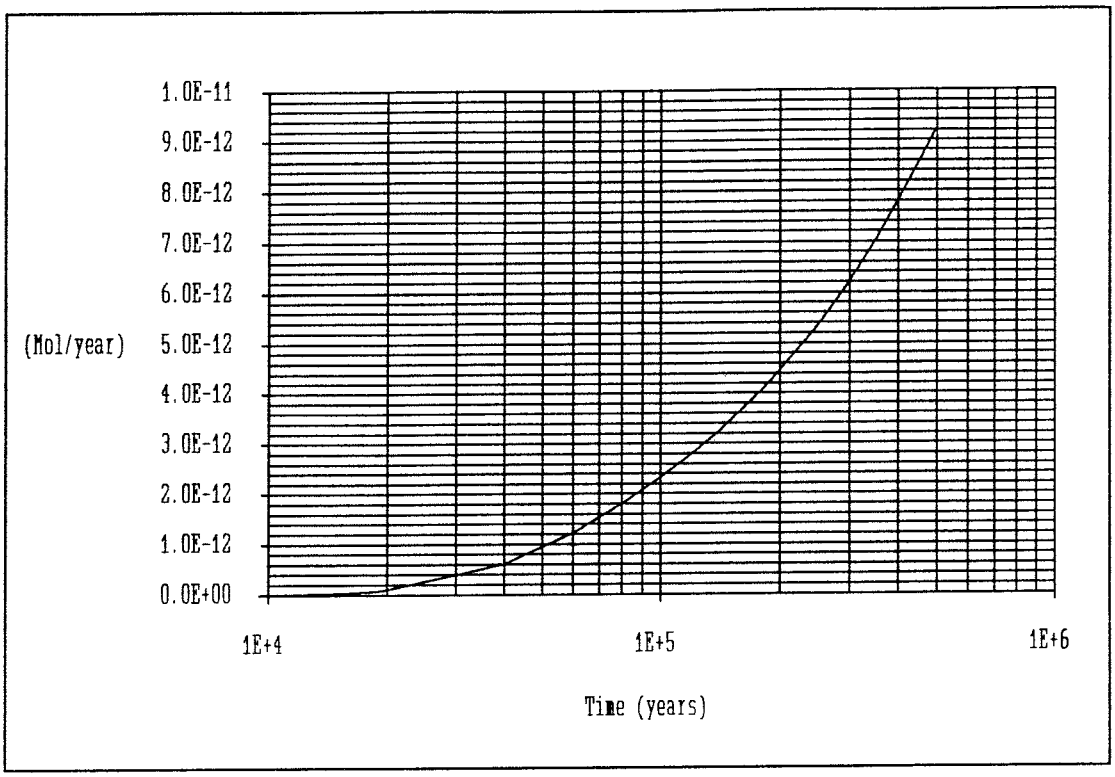

Figure 37
Release rate

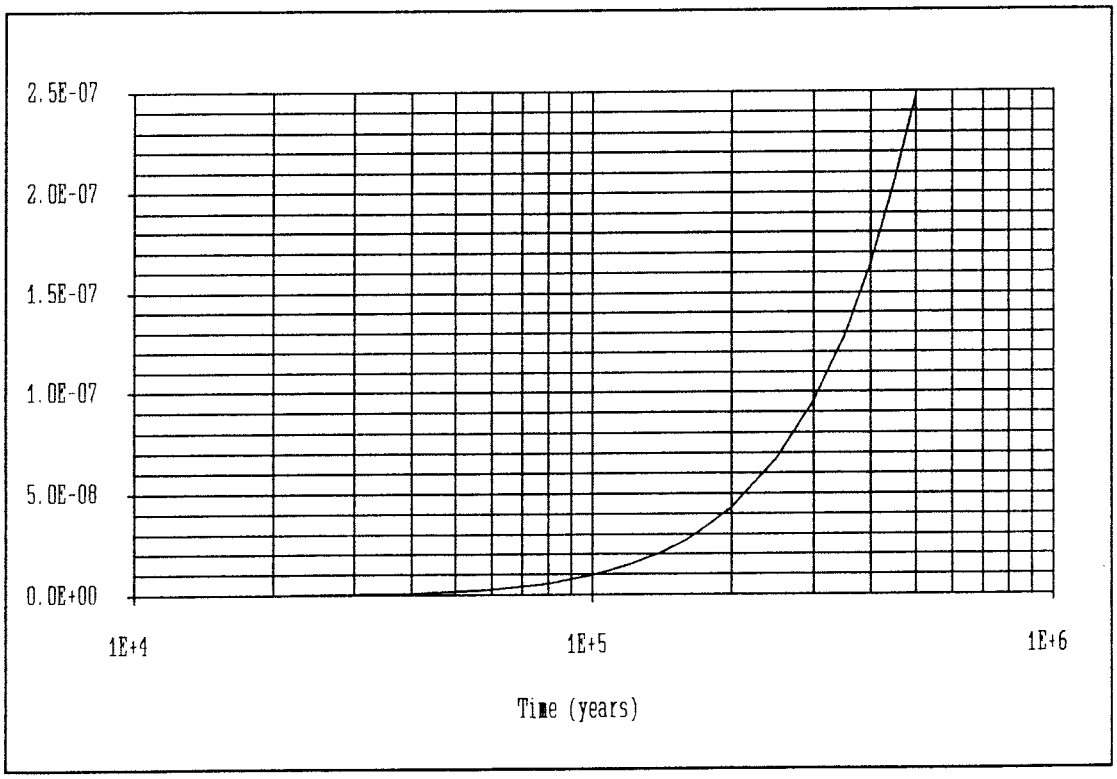

Figure 38
Released fraction.

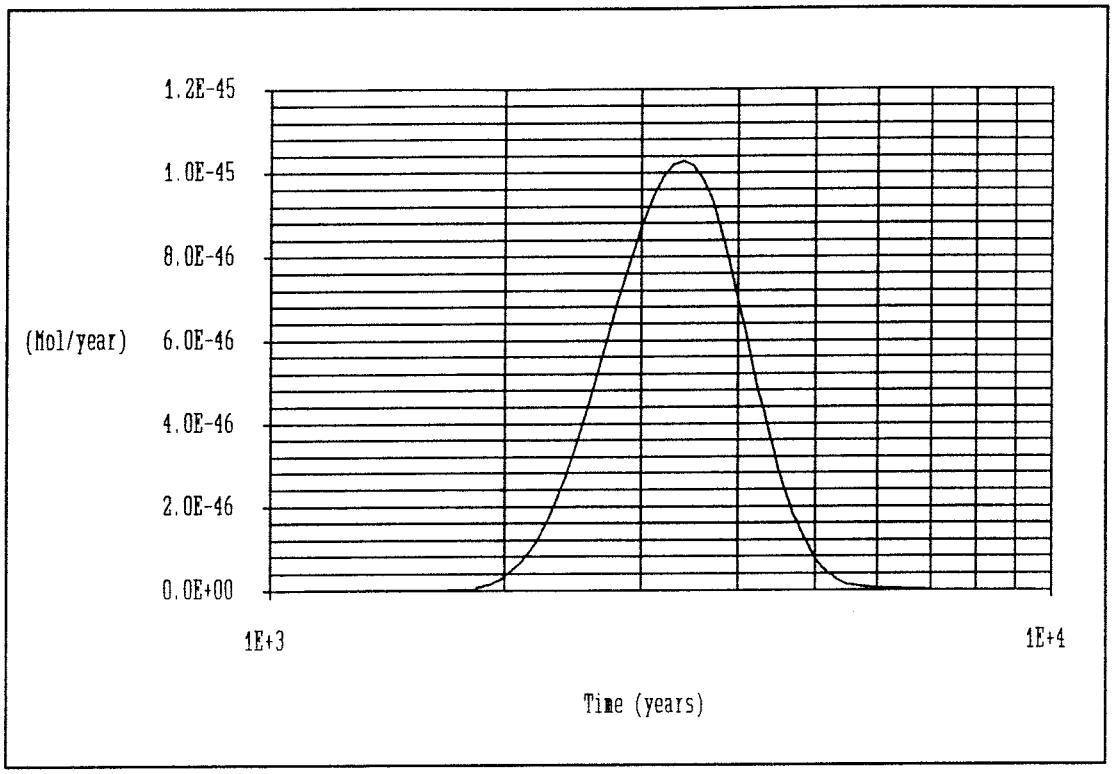

Figure 39
Release rate

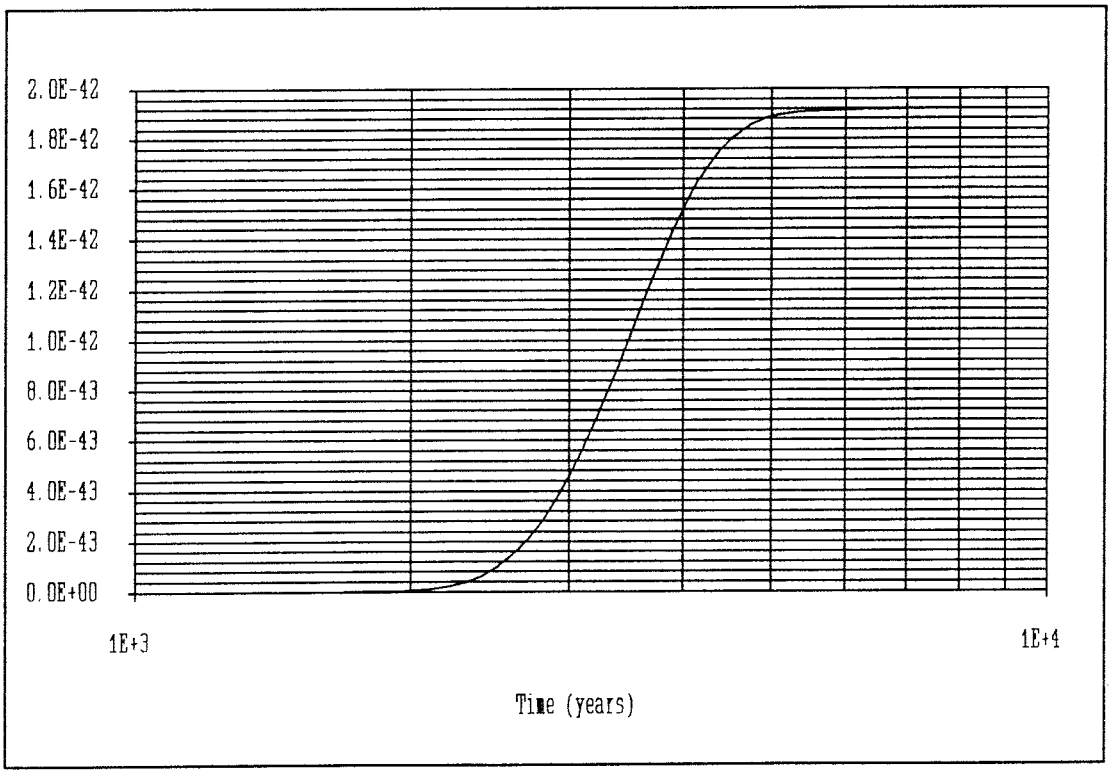

Figure 40
Released fraction.

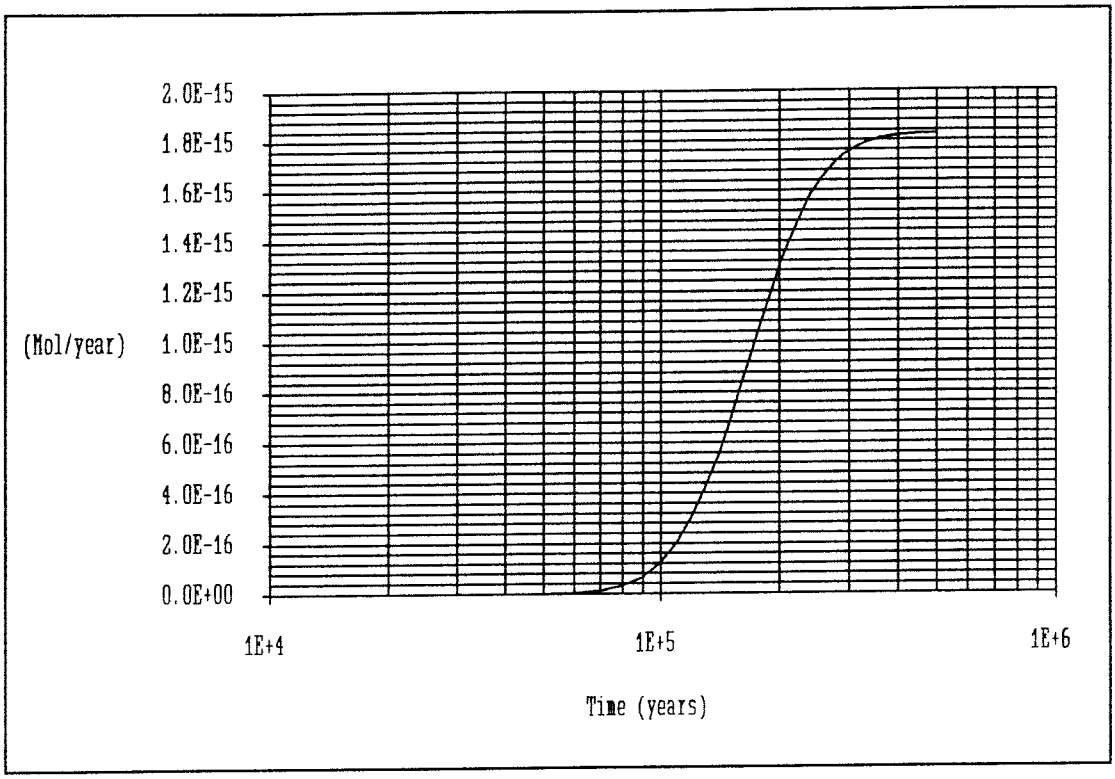

Figure 41
Release rate

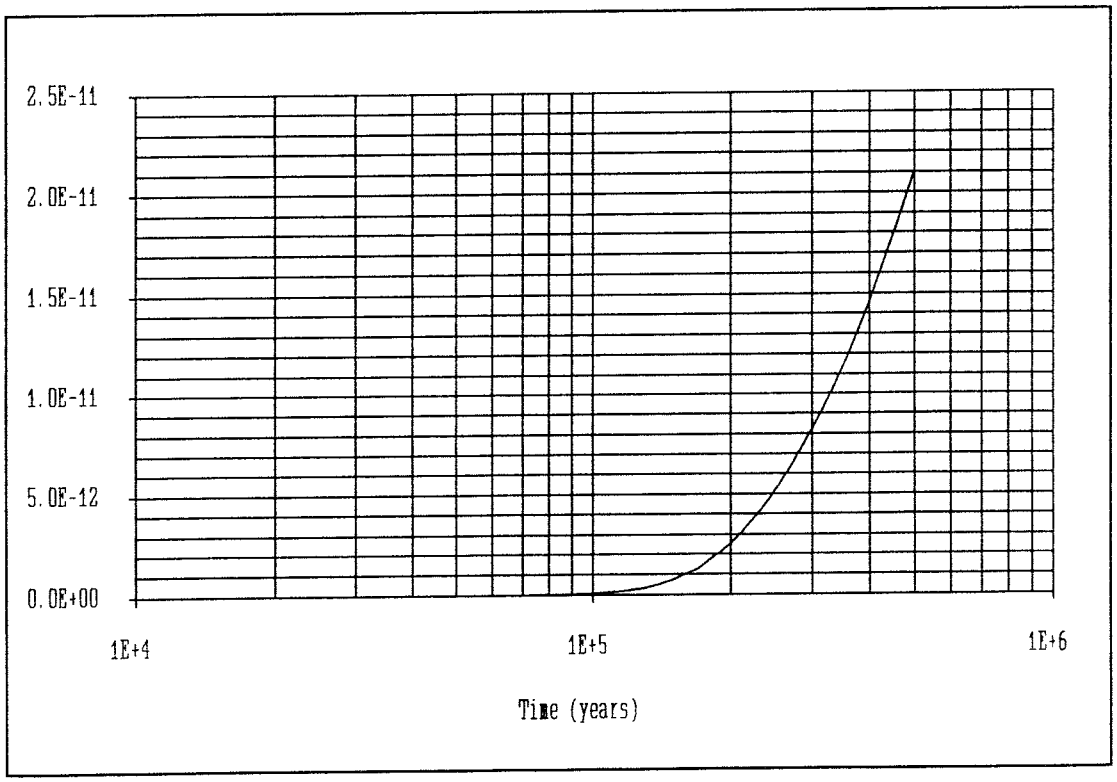

Figure 42
Released fraction.

Pu-240

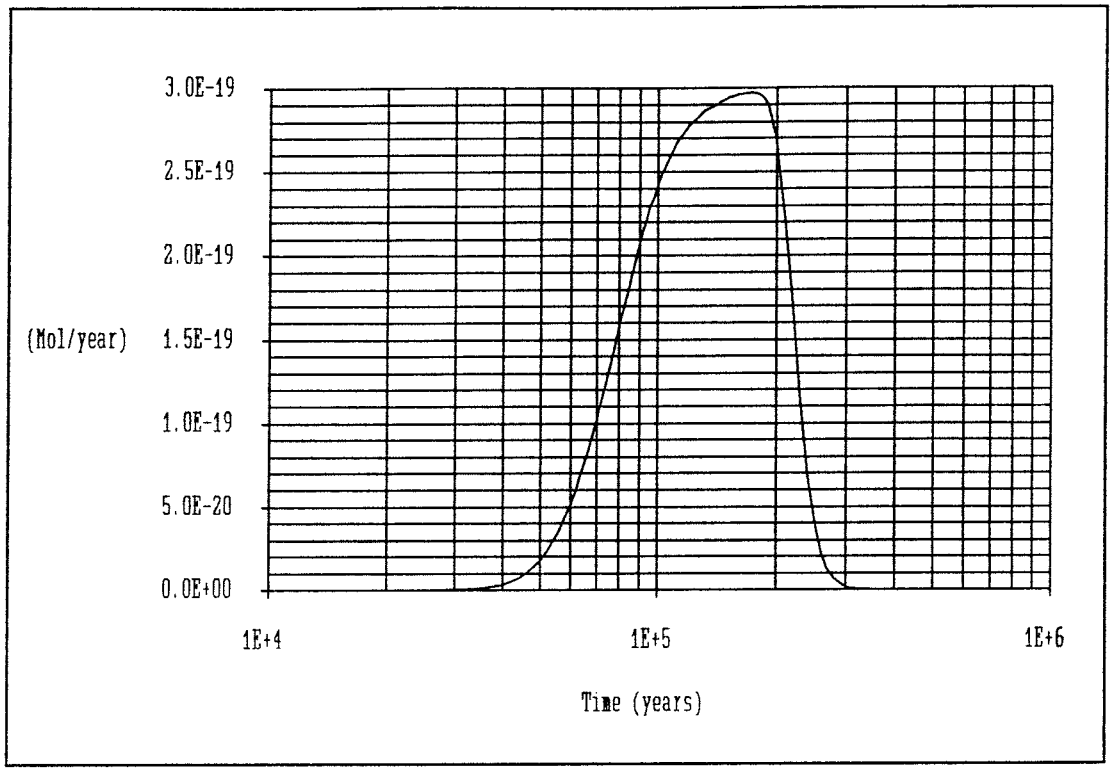

Figure 43
Release rate

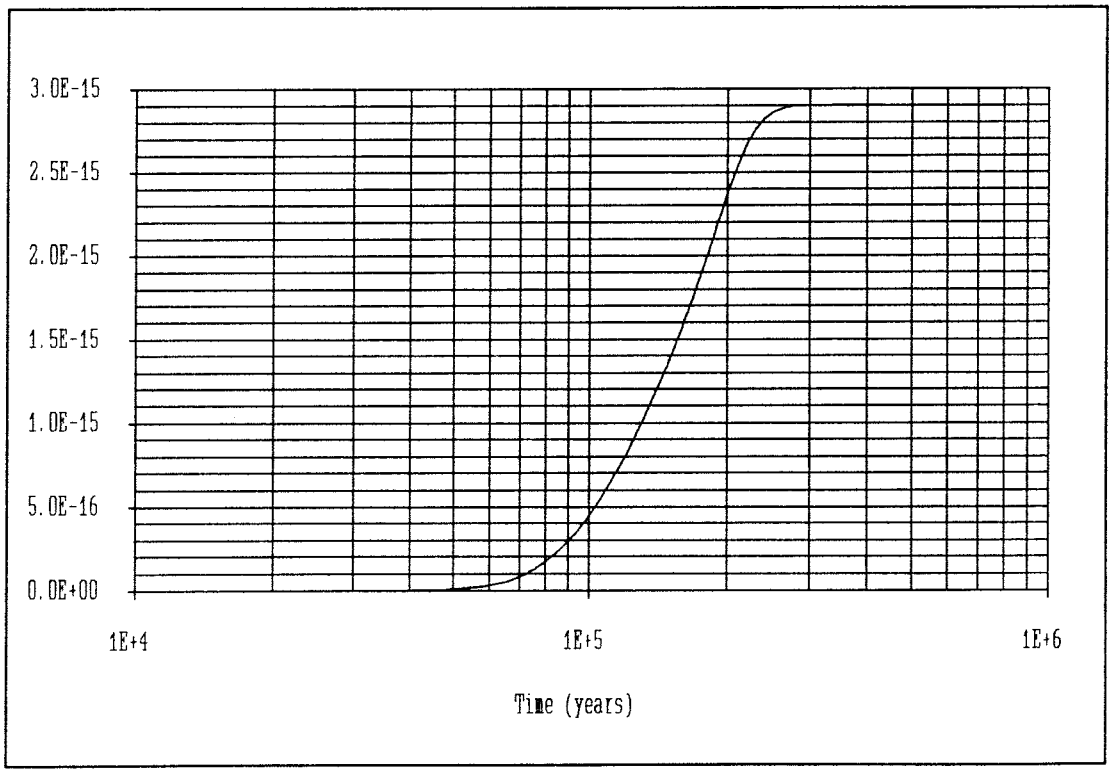

Figure 44
Released fraction.

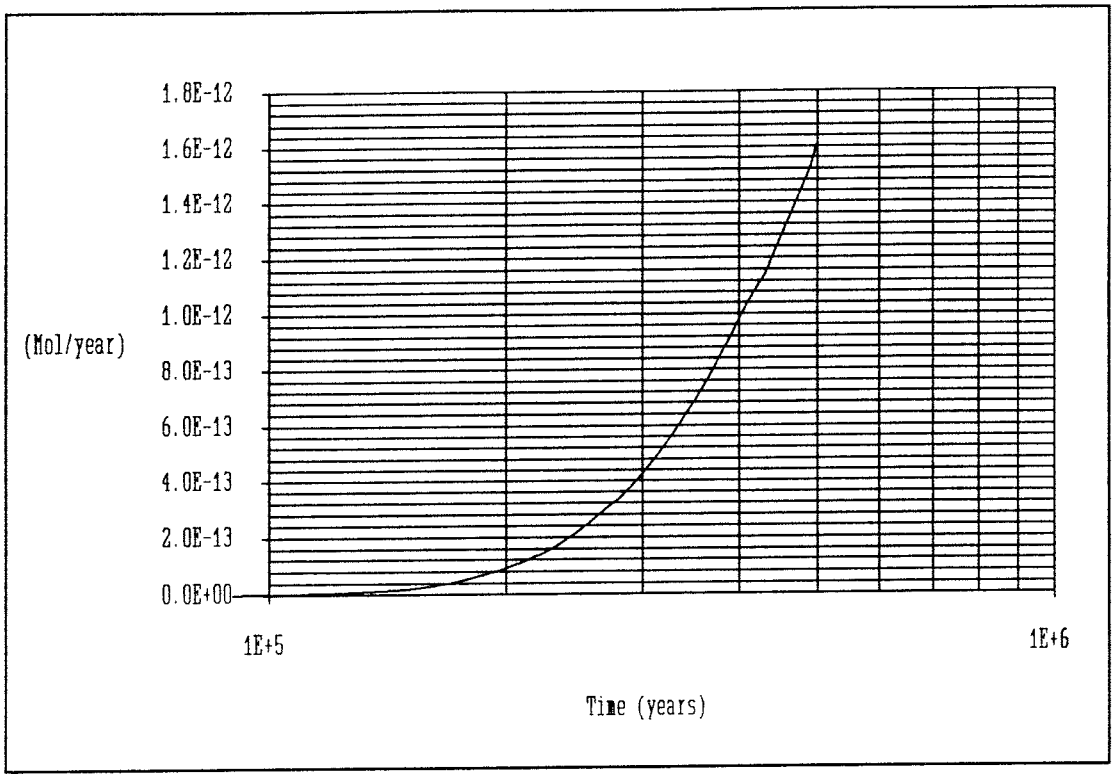

Figure 45
Release rate

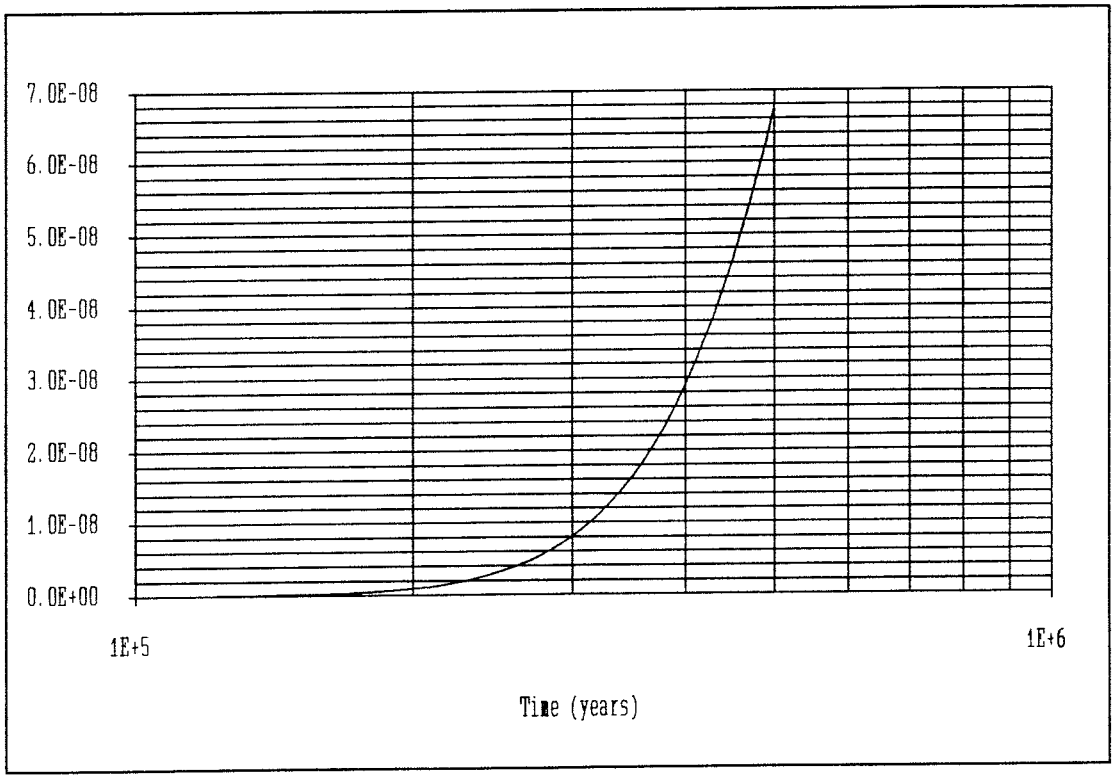

Figure 46
Released fraction.

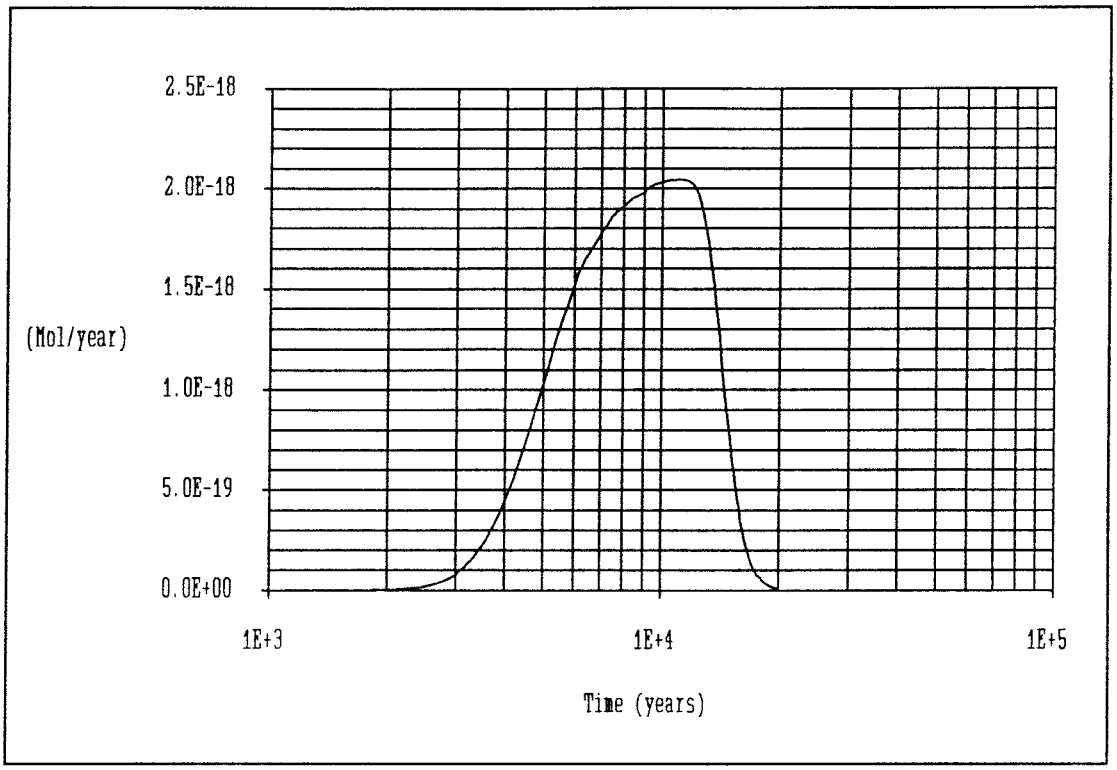

Figure 47
Release rate

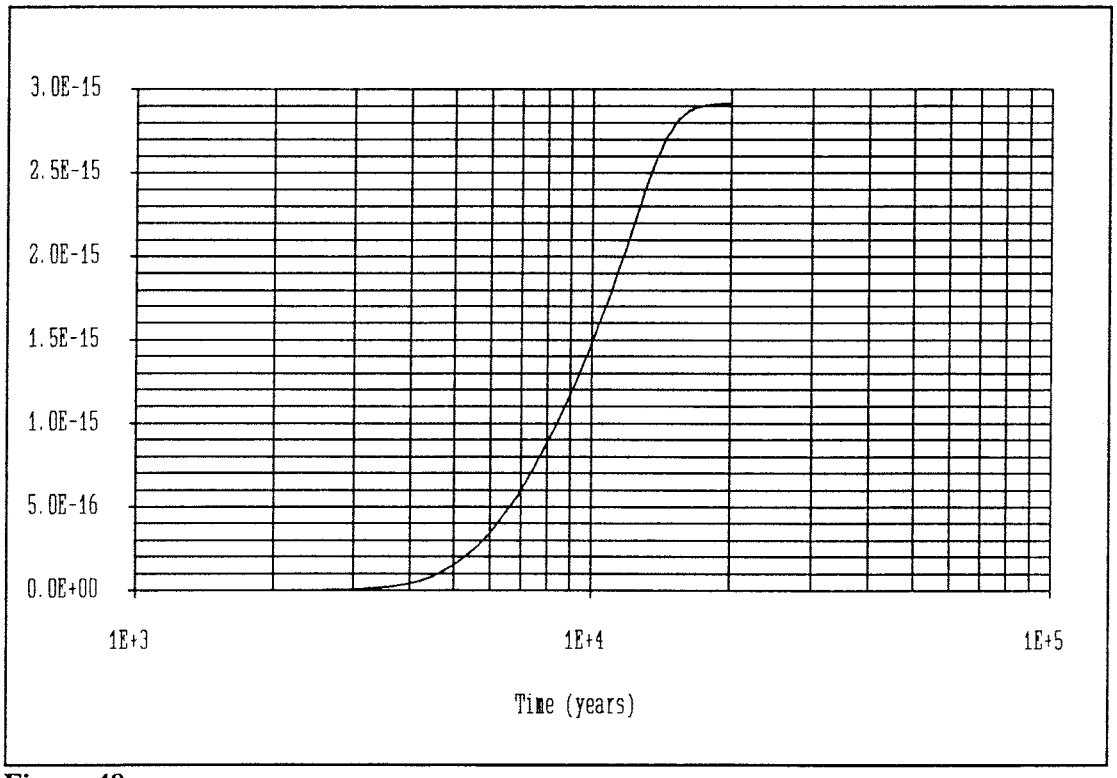

Figure 48
Released fraction.

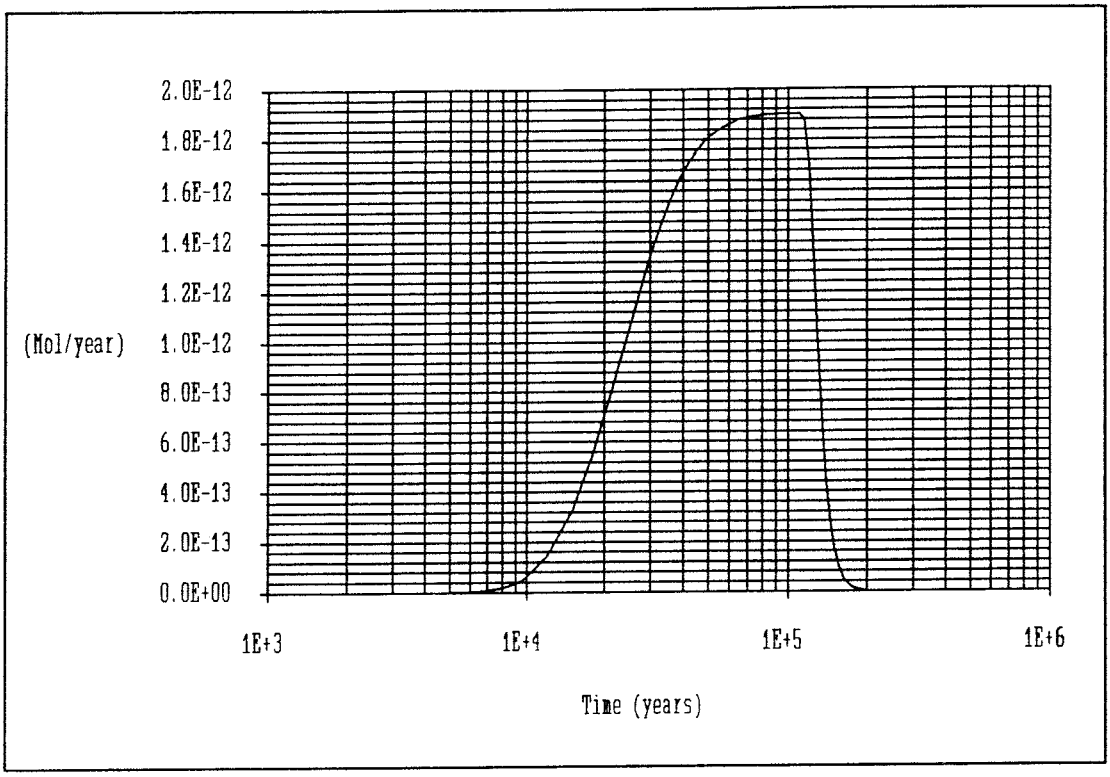

Figure 49
Release rate

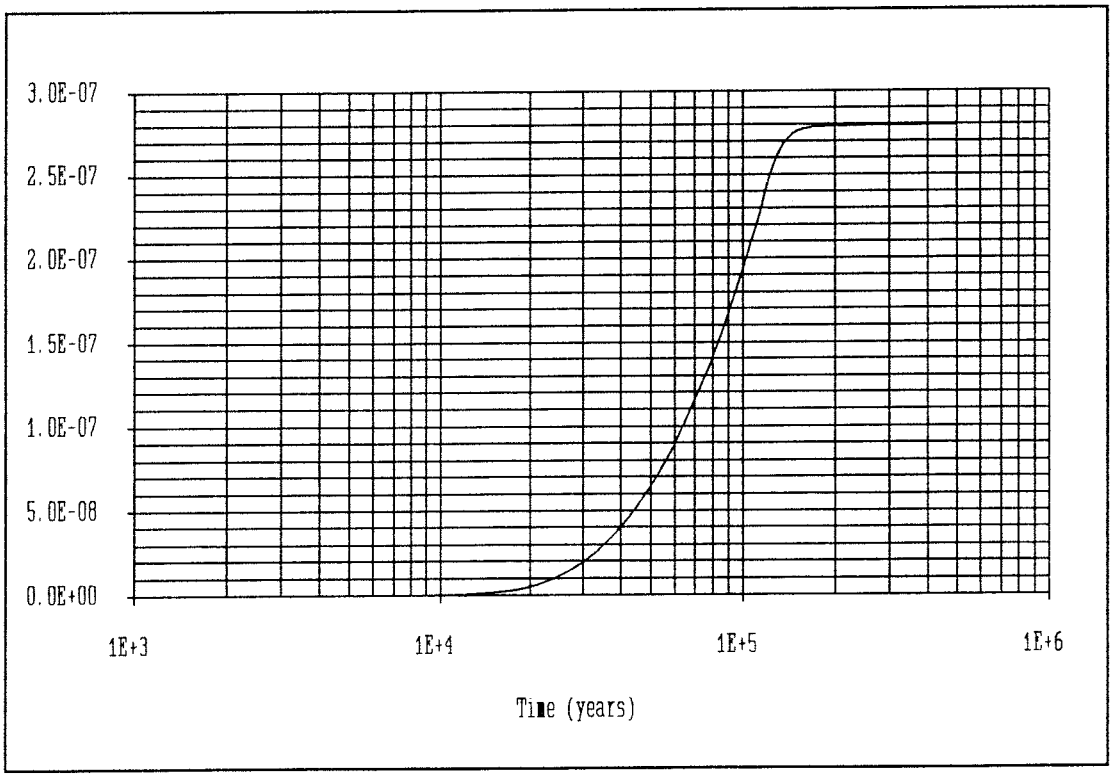

Figure 50
Released fraction.

Appendix B

The runtime structure of the Integrated Finite Differences computer calculations.

All the work has been performed on the SKB Convex C210 computer and all data- and program files except the IFD code TRUCHN reside on /files/home/users/kemab/0236 with subdirectories.

The version of the TRUCHN code used /files/home/users/kemab/truchn/truchn is an updimensioned but otherwise identical variant of the code on /usr/local/truchn/src.

The file structure consists of a small number of common data files on the project root directory. Under this directory is then a separate subdirectory for each of the nuclides. The name of these directories are the nuclide names written in small letters without a hyphen (e.g. c14, sn126, etc.) For the variations using a film resistance of 1, 9 and 99 times the resistance in the final part of the bentonite are created the subdirectories ni59a, ni59b and ni59c respectively.

The TRUCHN calculations were performed in a rather standardised way. Two shell script templates, also containing the nuclide specific parts of the input data were used. One for the solubility limited nuclides and one for the non solubility limited nuclides. The appropriate shell script template was copied to the nuclide subdirectory, the proper nuclide dependent data where inserted with a text editor and the shell script was started.

The general structure of the shell script was:
- Assemble a TRUCHN input data deck using the nuclide dependent data inserted into it and the data files on the project root directory common to all the runs (mostly discretisation data).
- Start the TRUCHN calculation
- Perform an extraction of the relevant output data from the voluminous TRUCHN output data file.
- Delete the TRUCHN output file (to preserve space on the disk)

The shell script for a certain run was renamed to "n.rtr" where n was a number from 1 and up. All the files created by running the shell script retain this number with different extensions for the different files. The date and time when the shell script last was run was written to the secondary output data files.

File name extensions used:

.rtr	Originating shell script file.
.inp	TRUCHN input data file.
.out	TRUCHN main output data file.
.dmp	TRUCHN dump of all node concentrations at restart.
.pu1	TRUCHN output data file of boundary connection nuclide fluxes.
.run	Short diagnostic printouts from the TRUCHN run
.txt	Stripped output data file with boundary connection nuclide fluxes for exportation to local computer for presentation.

Data files common to all runs:
block4, block5.2, block5.nuc, block6, block7.
(basdata.txt is a copy of the common spreadsheet table containing all the nuclide dependent input data together with a number of derived figures.)

List of SKB reports

Annual Reports

1977-78
TR 121
KBS Technical Reports 1 – 120
Summaries
Stockholm, May 1979

1979
TR 79-28
The KBS Annual Report 1979
KBS Technical Reports 79-01 – 79-27
Summaries
Stockholm, March 1980

1980
TR 80-26
The KBS Annual Report 1980
KBS Technical Reports 80-01 – 80-25
Summaries
Stockholm, March 1981

1981
TR 81-17
The KBS Annual Report 1981
KBS Technical Reports 81-01 – 81-16
Summaries
Stockholm, April 1982

1982
TR 82-28
The KBS Annual Report 1982
KBS Technical Reports 82-01 – 82-27
Summaries
Stockholm, July 1983

1983
TR 83-77
The KBS Annual Report 1983
KBS Technical Reports 83-01 – 83-76
Summaries
Stockholm, June 1984

1984
TR 85-01
Annual Research and Development Report 1984
Including Summaries of Technical Reports Issued during 1984. (Technical Reports 84-01 – 84-19)
Stockholm, June 1985

1985
TR 85-20
Annual Research and Development Report 1985
Including Summaries of Technical Reports Issued during 1985. (Technical Reports 85-01 – 85-19)
Stockholm, May 1986

1986
TR 86-31
SKB Annual Report 1986
Including Summaries of Technical Reports Issued during 1986
Stockholm, May 1987

1987
TR 87-33
SKB Annual Report 1987
Including Summaries of Technical Reports Issued during 1987
Stockholm, May 1988

1988
TR 88-32
SKB Annual Report 1988
Including Summaries of Technical Reports Issued during 1988
Stockholm, May 1989

1989
TR 89-40
SKB Annual Report 1989
Including Summaries of Technical Reports Issued during 1989
Stockholm, May 1990

Technical Reports

List of SKB Technical Reports 1991

TR 91-01
Description of geological data in SKB's database GEOTAB
Version 2
Stefan Sehlstedt, Tomas Stark
SGAB, Luleå
January 1991

TR 91-02
Description of geophysical data in SKB database GEOTAB
Version 2
Stefan Sehlstedt
SGAB, Luleå
January 1991

TR 91-03
1. The application of PIE techniques to the study of the corrosion of spent oxide fuel in deep-rock ground waters
2. Spent fuel degradation
R S Forsyth
Studsvik Nuclear
January 1991

TR 91-04
Plutonium solubilities
I Puigdomènech[1], J Bruno[2]
[1]Enviromental Services, Studsvik Nuclear, Nyköping, Sweden
[2]MBT Tecnologia Ambiental, CENT, Cerdanyola, Spain
February 1991

TR 91-05
Description of tracer data in the SKB database GEOTAB
SGAB, Luleå
April, 1991

TR 91-06
Description of background data in the SKB database GEOTAB
Version 2
Ebbe Eriksson, Stefan Sehlstedt
SGAB, Luleå
March 1991

TR 91-07
Description of hydrogeological data in the SKB's database GEOTAB
Version 2
Margareta Gerlach[1], Bengt Gentzschein[2]
[1]SGAB, Luleå
[2]SGAB, Uppsala
April 1991

TR 91-08
Overview of geologic and geohydrologic conditions at the Finnsjön site and its surroundings
Kaj Ahlbom[1], Sven Tirén[2]
[1]Conterra AB
[2]Sveriges Geologiska AB
January 1991

TR 91-09
Long term sampling and measuring program. Joint report for 1987, 1988 and 1989. Within the project: Fallout studies in the Gideå and Finnsjö areas after the Chernobyl accident in 1986
Thomas Ittner
SGAB, Uppsala
December 1990

TR 91-10
Sealing of rock joints by induced calcite precipitation. A case study from Bergeforsen hydro power plant
Eva Hakami[1], Anders Ekstav[2], Ulf Qvarfort[2]
[1]Vattenfall HydroPower AB
[2]Golder Geosystem AB
January 1991

TR 91-11
Impact from the disturbed zone on nuclide migration – a radioactive waste repository study
Akke Bengtsson[1], Bertil Grundfelt[1], Anders Markström[1], Anders Rasmuson[2]
[1]KEMAKTA Konsult AB
[2]Chalmers Institute of Technology
January 1991

TR 91-12
Numerical groundwater flow calculations at the Finnsjön site
Björn Lindbom, Anders Boghammar, Hans Lindberg, Jan Bjelkås
KEMAKTA Consultants Co, Stockholm
February 1991

TR 91-13
Discrete fracture modelling of the Finnsjön rock mass
Phase 1 feasibility study
J E Geier, C-L Axelsson
Golder Geosystem AB, Uppsala
March 1991

TR 91-14
Channel widths
Kai Palmqvist, Marianne Lindström
BERGAB-Berggeologiska Undersökningar AB
February 1991

TR 91-15
Uraninite alteration in an oxidizing environment and its relevance to the disposal of spent nuclear fuel
Robert Finch, Rodney Ewing
Department of Geology, University of New Mexico
December 1990

TR 91-16
Porosity, sorption and diffusivity data compiled for the SKB 91 study
Fredrik Brandberg, Kristina Skagius
Kemakta Consultants Co, Stockholm
April 1991

TR 91-17
Seismically deformed sediments in the Lansjärv area, Northern Sweden
Robert Lagerbäck
May 1991

TR 91-18
Numerical inversion of Laplace transforms using integration and convergence acceleration
Sven-Åke Gustafson
Rogaland University, Stavanger, Norway
May 1991

TR 91-19
NEAR21 - A near field radionuclide migration code for use with the PROPER package
Sven Norman[1], Nils Kjellbert[2]
[1]Starprog AB
[2]SKB AB
April 1991

TR 91-20
Äspö Hard Rock Laboratory. Overview of the investigations 1986-1990
R Stanfors, M Erlström, I Markström
June 1991

TR 91-21
Äspö Hard Rock Laboratory. Field investigation methodology and instruments used in the pre-investigation phase, 1986-1990
K-E Almén, O Zellman
June 1991

TR 91-22
Äspö Hard Rock Laboratory. Evaluation and conceptual modelling based on the pre-investigations 1986-1990
P Wikberg, G Gustafson, I Rhén, R Stanfors
June 1991

TR 91-23
Äspö Hard Rock Laboratory. Predictions prior to excavation and the process of their validation
Gunnar Gustafson, Magnus Liedholm, Ingvar Rhén, Roy Stanfors, Peter Wikberg
June 1991

TR 91-24
Hydrogeological conditions in the Finnsjön area. Compilation of data and conceptual model
Jan-Erik Andersson, Rune Nordqvist, Göran Nyberg, John Smellie, Sven Tirén
February 1991

TR 91-25
The role of the disturbed rock zone in radioactive waste repository safety and performance assessment. A topical discussion and international overview.
Anders Winberg
June 1991

TR 91-26
Testing of parameter averaging techniques for far-field migration calculations using FARF31 with varying velocity.
Akke Bengtsson[1], Anders Boghammar[1], Bertil Grundfelt[1], Anders Rasmuson[2]
[1]KEMAKTA Consultants Co
[2]Chalmers Institute of Technology

TR 91-27
Verification of HYDRASTAR. A code for stochastic continuum simulation of groundwater flow
Sven Norman
Starprog AB
July 1991

TR 91-28
Radionuclide content in surface and groundwater transformed into breakthrough curves. A Chernobyl fallout study in an forested area in Northern Sweden
Thomas Ittner, Erik Gustafsson, Rune Nordqvist
SGAB, Uppsala
June 1991

TR 91-29
Soil map, area and volume calculations in Orrmyrberget catchment basin at Gideå, Northern Sweden
Thomas Ittner, P-T Tammela, Erik Gustafsson
SGAB, Uppsala
June 1991

TR 91-30
A resistance network model for radionuclide transport into the near field surrounding a repository for nuclear waste (SKB, Near Field Model 91)
Lennart Nilsson, Luis Moreno, Ivars Neretnieks, Leonardo Romero
Department of Chemical Engineering,
Royal Institute of Technology, Stockholm
June 1991

TR 91-31

Near field studies within the SKB 91 project

Hans Widén, Akke Bengtsson, Bertil Grundfelt
Kemakta Consultants AB, Stockholm

June 1991

TR 91-32

SKB/TVO Ice age scenario

Kaj Ahlbom[1], Timo Äikäs[2], Lars O. Ericsson[3]
[1]Conterra AB
[2]Teollisuuden Voima Oy (TVO)
[3]Svensk Kärnbränslehantering AB (SKB)

June 1991